Received: 9 December 2019 | Revised: 6 March 2020 | Accepted: 17 March 2020

DOI: 10.1002/dep2.110

ORIGINAL RESEARCH ARTICLE

The Depositional Record Open Access
A journal of the International Association of Sedimentologists
WILEY

Engraved on the rocks—Aeolian abrasion of Martian mudstone exposures and their relationship to modern wind patterns in Gale Crater, Mars

Juergen Schieber[1] | **Michelle E. Minitti**[2] | **Robert Sullivan**[3] | **Kenneth S. Edgett**[4] | **Michael C. Malin**[4] | **Tim Parker**[5] | **Fred Calef**[5]

[1]Department of Geological Sciences, Indiana University, Bloomington, IN, USA

[2]Framework, Silver Spring, MD, USA

[3]CCAPS, Cornell University, Ithaca, NY, USA

[4]Malin Space Science Systems, San Diego, CA, USA

[5]JPL, Pasadena, CA, USA

Correspondence
Juergen Schieber, Department of Geological Sciences, Indiana University, Bloomington, IN, USA.
Email: jschiebe@indiana.edu

Funding information
Indiana University Shale Research Consortium; NASA, Grant/Award Number: 1516826

Abstract

In this contribution we report measurements and interpretations of aeolian abrasion features observed along the Mars Science Laboratory rover traverse at Gale Crater on Mars. Aeolian abrasion of surface rocks has been documented by most missions that have landed on Mars, but attention has largely focused on relatively resistant rocks that display ventifact morphologies well-known from Earth. The current study instead emphasizes abrasion features developed on mudstone surfaces, because aeolian abrasion textures are very common in the mudstone-dominated Murray Formation at Gale Crater. These abrasion textures have been observed over a wide area, and they allow deductions about dominant past wind regimes that differ from those observed at present. On Earth, aeolian abrasion features in mudstone outcrops have minimal preservation potential because of the susceptibility of mudstones to moisture and aqueous erosion, even in dominantly arid surface environments. Because of this there is no literature on potential terrestrial analogs. In order to better understand aeolian abrasion morphologies in mudstones on Mars, laboratory experiments were conducted that exposed a range of mudstone samples and rock simulant samples to wind-driven sand for periods of up to four months. These experiments produced a range of aeolian abrasion textures ('wind tails', fluting, differential 'etching' of laminae, stalks and pedestals) that can serve as analogs for features in the Murray Formation, increasing our confidence regarding aeolian origins for these and the deductions of formative, sand-driving wind azimuths. Orientations of aeolian abrasion textures along the Mars Science Laboratory traverse were compared with active ripple orientations in rover images, and with previous analyses of orbital images of the study area, in order to evaluate whether the current, complex wind environment can explain the abrasion orientations observed in rover images, or if the abrasion record might also contain signatures of past wind regimes that differed from those of the present. Results show relatively coherent patterns of airflow and sand movement that vary in accordance with factors like local topography and upwind availability

of sand for abrasion. Wind events blowing southwest that are primarily responsible for southwest migration of the Bagnold Dunes have also caused bedrock abrasion of similar orientation between these dunes. Less effective wind events (from an abrasion standpoint) blowing south-southeast have broadly affected bedrock exposures elsewhere across the Mars Science Laboratory landing site away from the Bagnold Dunes. A notable exception are northeast abrasion textures on the more erosion-resistant sandstones of the Naukluft Plateau. The latter are consistent with one of two abrasion directions measured in previous studies, prior to the rover's arrival at the Murray Formation mudstones, and probably reflect the preservation of an ancient sand-driving wind regime that differs from that of the present.

KEYWORDS

Aeolian abrasion, experiment, Mars, mudstone, wind patterns

1 | INTRODUCTION

Orbital imaging surveys of Mars have revealed geomorphic and geochemical evidence for water early in the planet's history, including ancient valley networks and phyllosilicate-bearing rock (Carr, 1996; Malin and Edgett, 2000; Bibring *et al*., 2006; Carr and Head, 2010). The last half of the planet's history has been characterized by increased aridity (Carr and Head, 2010), when aeolian processes have played significant roles in sediment transport and shaping the planet's surface (Yen *et al.*, 2005; Urso *et al.*, 2018; and many others). The Mars Science Laboratory (MSL) *Curiosity* rover landed in the 154 km diameter Gale Crater in August 2012 to survey a suite of ancient sedimentary rocks that were considered to have high potential for providing crucial insights about a planet-wide transition to more consistently arid conditions (Grotzinger *et al.*, 2012). The rover traverse, along which the data for this study were collected, is approximately 20 km long (to date) and has explored an approximately 350 m thick stack of sedimentary rocks (Figure 1).

Since landing, the MSL rover has been used to observe numerous examples of rock surfaces that have been abraded by wind-driven particles (Bridges *et al.*, 2014; Schieber *et al.*, 2017), adding to the record of aeolian abrasion observed at other lander and rover sites on Mars (Sharp and Malin, 1984; Bridges *et al.*, 1999; Greeley *et al.*, 2002; 2004; 2006; 2008; Sullivan *et al.*, 2005; Herkenhoff *et al.*, 2008; Thomson *et al.*, 2008). For example, Figure 1 shows MSL rover views of aeolian abrasion textures on the Sheepbed mudstone (Grotzinger, 2014; Day and Kocurek, 2016; Schieber *et al.*, 2017), and on the mudstone-dominated Murray Formation (Grotzinger *et al.*, 2015; Rampe *et al.*, 2017) at Gale Crater. Abrasion textures such as these 'wind tails' (Figure 1) require two conditions: (a) rock bodies having inclusions (of sedimentary, volcanic or diagenetic origin) with greater resistance to aeolian abrasion than their host materials; and (b) wind-driven sand impacting the target rock along a single, consistent azimuth. In this sense, aeolian abrasion textures do not necessarily record the strongest or most common wind direction, because the amount of sand available upwind along any particular wind azimuth is an important factor. Wind abrasion orientations can also record influences from nearby obstacles blocking or re-directing low-angle saltating sand trajectories as sand nears the target rock surface. Consequently, important regional wind azimuths that lack an upwind sand supply (including wind azimuths that might even be strongest, or most common), or that correspond to sand delivery azimuths blocked by local obstacles, will not be recorded by abrasion textures on the target rock surface. In cases where local obstacles block sand saltating from the most effective regional sand-abrading azimuth, the target rock might instead record abrasion from a secondary or minor sand migration direction that would be undetectable in more exposed areas where primary sand pathways establish aeolian abrasion textures on rock surfaces. Notwithstanding these potential complications, abrasion textures such as those in Figure 1 still have the potential to document regional sand transport azimuths along the MSL rover traverse at Gale Crater, but two questions must be addressed: (a) Do abrasion orientations measured along the rover traverse represent a coherent, regional picture of wind-driven sand motions, despite possible local effects from topography and nearby obstacles influencing sand pathways to individual target rocks? (b) If so, are abrasion directions consistent with present-day regional wind conditions and azimuths upwind to current sand sources, or might the rock abrasion record be more complex, indicating contributions also from different wind conditions and/or sand sources from an earlier epoch?

Wind abrasion features such as those in Figure 1 are common in MSL images of the Murray Formation obtained with

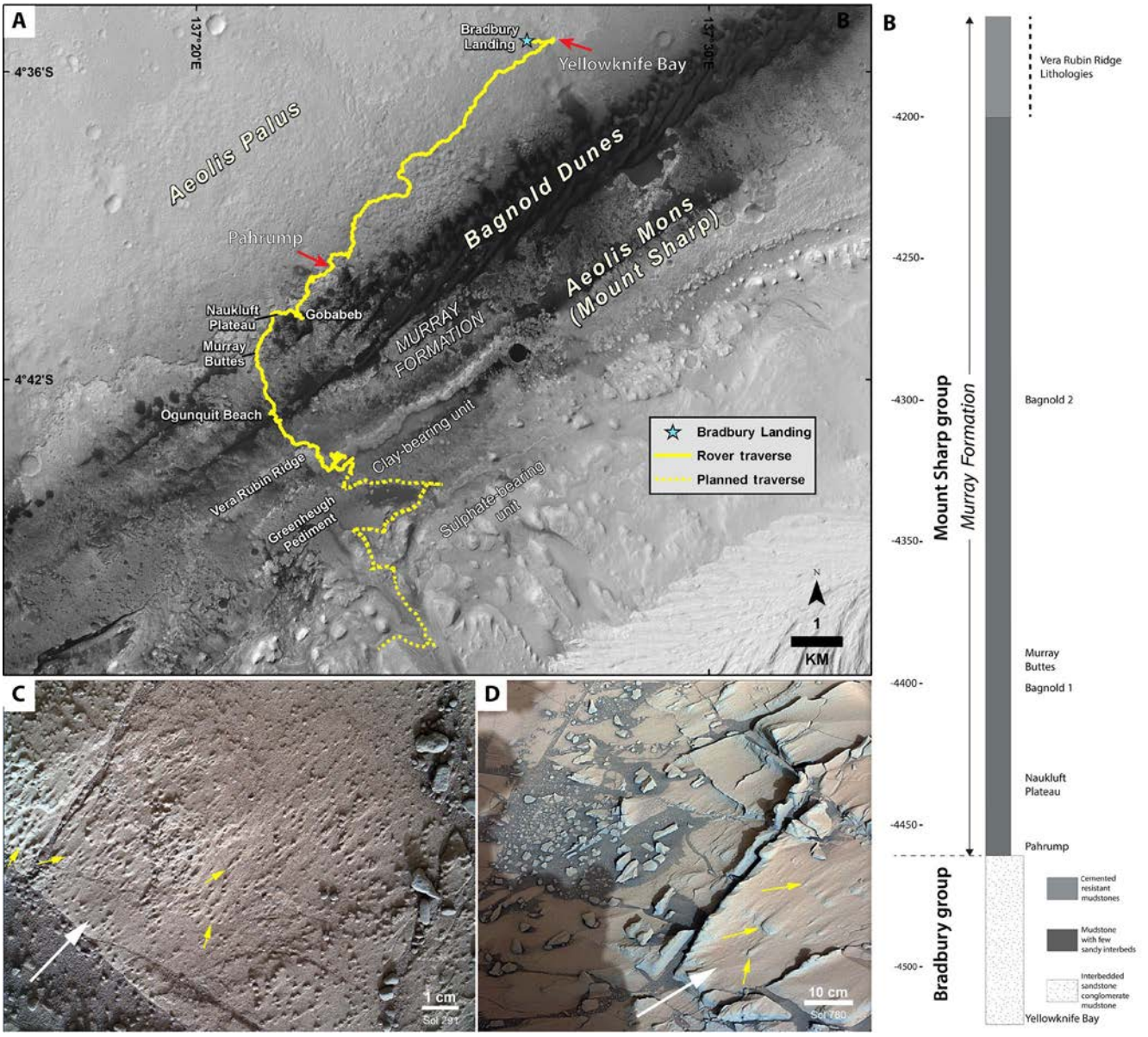

FIGURE 1 (A) Context map (https://photojournal.jpl.nasa.gov/jpeg/PIA23412.jpg) and rover traverse with landmarks noted in text. (B) Simplified column presentation of the rocks encountered by the rover as it ascended Mount Sharp (formally known as Aeolis Mons). The lower interval is the Bradbury Group (interstratified sandstone, conglomerates and mudstones), and the upper interval is the Mount Sharp Group which at this stage of exploration consists entirely of the Murray Formation (dominated by mudstones). The Murray Formation has been subdivided into members (Fedo *et al.*, 2017), but for the purposes of this study the fact that it consists largely of mudstones is sufficient. (C and D) Wind erosion features observed with (C) the arm-mounted MAHLI (Mars Hand Lens Imager) camera (image 0291MH0001970010103292C00), and (D) the 34 mm Mastcam (image 0780ML0034060040400309E01). Yellow arrows point to "wind tails" (Schieber *et al.*, 2017) produced by abrasive action of sand grains, white arrows indicate the probably direction of the wind. The locations for (C, Yellowknife Bay) and (D, Pahrump) are marked with red arrows on (A)

the mast-mounted Mastcam (Malin *et al.*, 2017), and the arm-mounted Mars Hand Lens Imager (MAHLI) camera (Edgett *et al.*, 2012). However, evaluating orientations of ground features from these images is complicated by distortions of perspective from oblique camera viewing angles and outcrop topography. A simpler, more efficient approach involves using the MARDI (Mars Descent Imager) camera (Malin *et al.*, 2017), because of this camera's fixed nadir pointing position (attached to the rover body) and constant ground area field of view. As long as the rover heading is known at the time of MARDI image acquisition, the orientation of surface features within the MARDI field of view is readily determined (Figure 2). Although MARDI's original purpose was to acquire images only during the rover's descent to the surface (see Moores *et al.*, 2016), it has since been operated routinely as a ground survey camera (Yingst *et al.*, 2013;

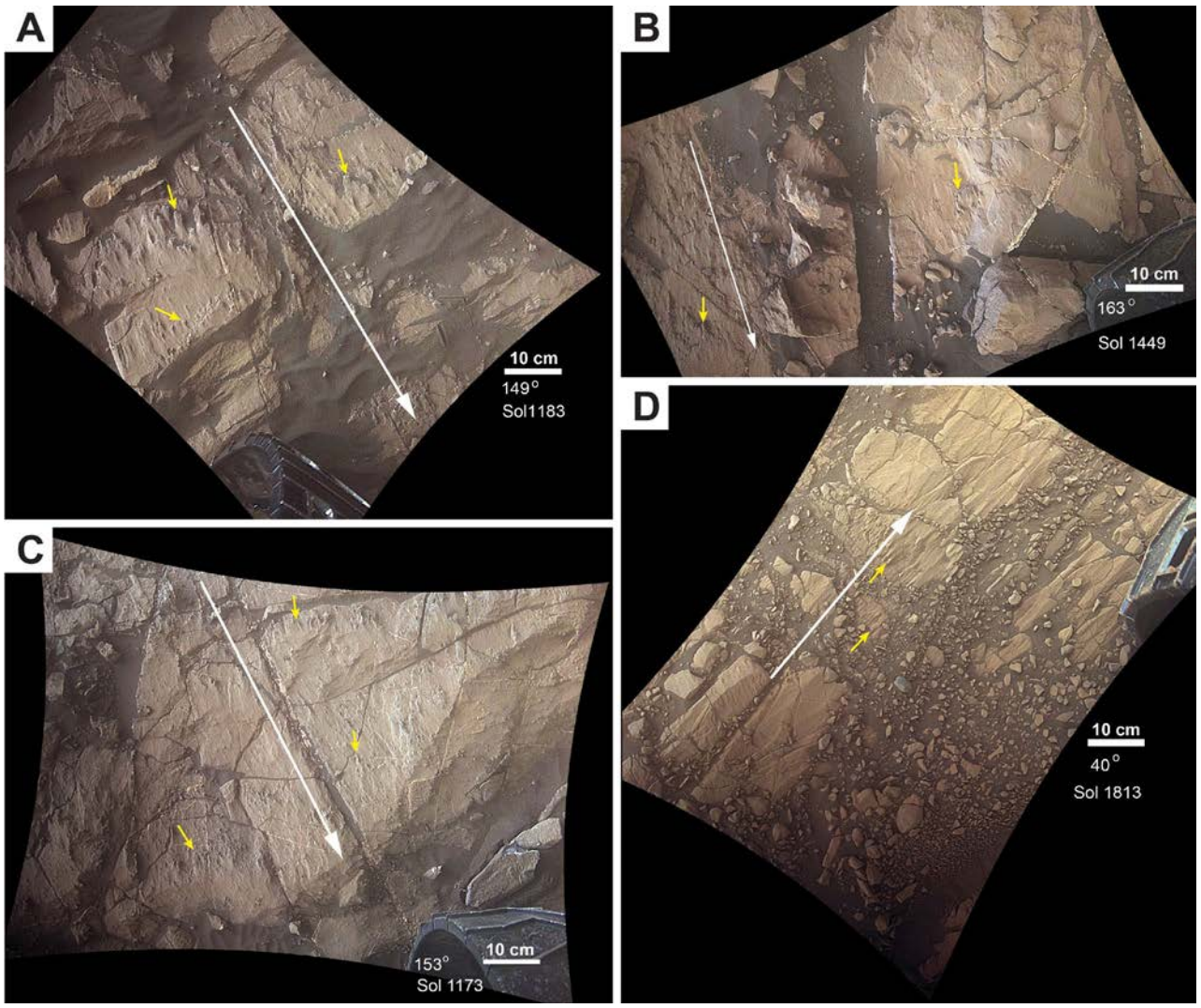

FIGURE 2 Examples of 'wind tails' at multiple locations, as seen via MARDI. The original images have been rotated so that they are oriented with North pointing up. The white arrows show interpreted wind directions, and the yellow arrows show 'wind tails' with stubby ends pointing upwind and sharper ends trailing downwind. The exact orientation of 'wind tails' can vary somewhat across the field of view, and the white arrow is an attempt to indicate the overall direction of interpreted airflow. The MARDI images are (A) 1183MD0004530000200391E01, (B) 1449MD0005480000200598E01, (C) 1173MD0004440000103756E01 and (D) 1813MD0007370000200783E01

Minitti *et al.*, 2017; 2019). For the purposes of this paper, use of MARDI images simplifies and standardizes procedures for sampling the orientations of aeolian features at rover locations along the traverse and mapping them over larger areas.

Aeolian abrasion is caused by the impact of saltating sand grains, which will have different erosive effects depending on rock type, impact angle and many other factors, resulting in a wide variety of erosionally carved rock shapes (ventifacts) and surface features such as flutes, grooves and pits (Maxson, 1940; Laity, 1994; Laity and Bridges, 2009). Abrasion features described as 'wind tails' have been reported from rocks examined at Meridiani Planum on Mars (Herkenhoff *et al*., 2008), and are morphologically very similar to those described from mudrocks in Gale Crater (Schieber *et al.*, 2017). Analogous features have also been reported from ignimbrites in Argentina (Favaro *et al.*, 2017). The authors, however, are unaware of reports of erosional wind tails in terrestrial mudstones. A probably explanation is that terrestrial mudstones are susceptible to degradation involving water, even in areas that receive very little rainfall. Aeolian abrasion textures may form on terrestrial mudstone surfaces intermittently, but even small amounts of precipitation will cause wetting, swelling and disintegration, and subsequent surface runoff will leave a fluvial imprint (Figure 3). Because it is therefore difficult to study the effects of aeolian abrasion in terrestrial mudstone exposures, a series of aeolian abrasion experiments were conducted on mudstone samples and experimental analogs (Howald and Schieber, 2008; Wilson *et al.*, 2011; Rossman *et al.*, 2012). The results of these experiments are used here to aid interpretation of features observed on Mars. Although this work does not have the benefit of petrographic information from thin sections of these Martian rocks, experimentally produced textural analogs can inform deductions regarding the degree

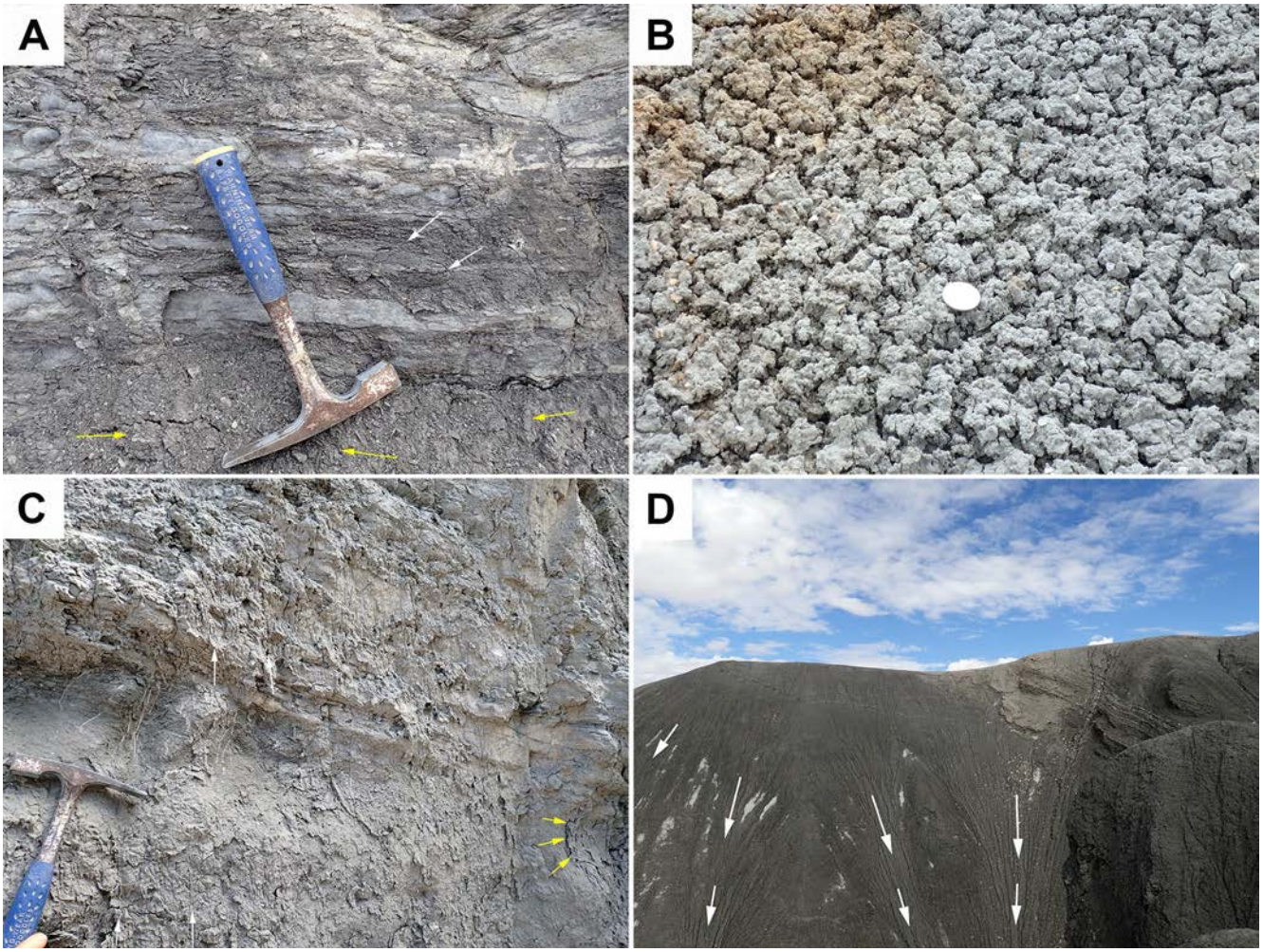

FIGURE 3 Mudstone weathering on Earth via examples from the Tununk Shale near Hanskville, Utah. (A) Relatively 'fresh' outcrop. Layering is visible, but moisture related shrinking and expansion has caused the rock to break into chips (white arrows) and accumulate below in a veneer of broken up debris (yellow arrows). (B) Further wetting and drying of this smectite-rich debris leads to 'popcorn' surface texture (coin for scale) that covers the underlying bedrock. (C) On steeper slopes occasional rain generates a muddy 'soup' that drips and flows across the surface (white arrows) and mantles the rock surface (yellow arrows). (D) Downslope gullies (white arrows) then cut into this soft substrate. Even though this is a desert, and there is wind and sand and potential for aeolian abrasion, moisture and infrequent rainfalls dominate degradation of the rock and surface morphology. Wind tails and related aeolian abrasion features, should they form, have minimal preservation potential

of cementation, compositional heterogeneity and relative rock hardness on Mars. Observations presented in this paper show that directional features related to aeolian abrasion correspond to long-term sand delivery azimuths and display considerable coherence over large areas. They reflect an interaction of near-surface airflow and sand transport pathways with topography, and preserve palaeowind patterns that probably have affected the lower slopes of Mount Sharp (Figure 1) for many millennia.

2 | METHODS

2.1 | Mudstone abrasion experiments

Laboratory experiments on wind erosion of mudstone specimens and experimental analogs (gypsum) employed a circular chamber with a motor-driven rotor that enabled sustained wind speeds of up to 60 km/hr (Figure 4). Erosion experiments were initially conducted with a variety of abrasives, such as powdered hematite (0.1 mm or smaller), crushed and sieved basalt (medium sand), and fine to medium quartz sand. Because all three abrasives produced comparable results, quartz sand was used in the majority of experiments (Wilson *et al.*, 2011; Rossman *et al.*, 2012). Abrasion experiments with a sustained wind speed of 30 km/hr lasted from several weeks to as long as four months, with occasional interruptions to examine specimens and record abrasion progress.

Samples were placed along the outer wall of the chamber (secured with Velcro pads, and oriented parallel to chamber bottom), and 1 kg of medium quartz sand was added as an abrasive. Because the sand simply moves in circles and interacts with a soft substrate, there is negligible loss and no further sand

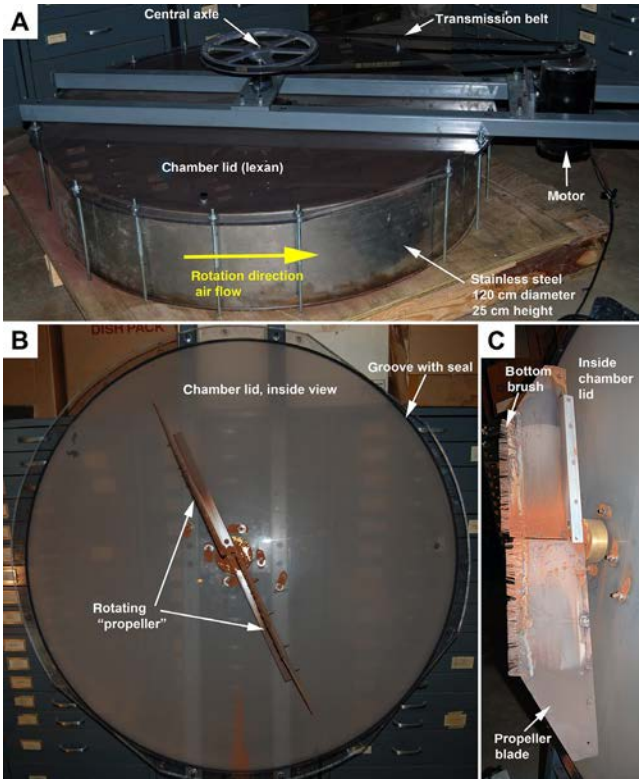

FIGURE 4 (A) The cylindrical chamber used for mudstone abrasion experiments. Chamber dimensions are 120 cm diameter, and 25 cm height. The chamber is covered with a fitted Lexan lid to which a speed controlled motor and a propeller shaft (central axle) has been attached. Steel bolts secure the lid to the underlying wooden platform and tighten it to the chamber top. (B) Inside view of the chamber lid that shows the central axle with propeller blades attached. The groove with foam seal fits the lid to the chamber. (C) Side view of the propeller shows propeller blades and a brush attached to the bottom of the blades. The brush prevents buildup of sand in the center of the chamber

needs to be added over the course of an experiment run. Wind speed was controlled by varying motor speed. Airflow velocity in the sample space was measured with a vane anemometer and calibrated to motor rpm. The lid plus propeller was removed for intermittent examination of abrasion progress. To prevent dust buildup on samples and in the chamber, the chamber air was passed through a vacuum cleaner twice daily.

Measurements of sand flux would be desirable for comparing these experiments to Mars conditions to assess the length of time that might be required to produce these features on present-day Mars. However, the experiment apparatus was not well-suited for this. In a linear abrasion setup where sand is fed at a constant rate through a known cross-section, estimates of sand flux are straightforward to derive. In the device used here, however, the sand is recirculated internally and may also become trapped intermittently in front of and on the lee sides of samples, making accurate flux determinations impracticable.

2.2 | Images from the Curiosity rover

The MARDI images used for this study were acquired generally under twilight conditions at each end-of-drive rover position. These late-day images provide better views of surface details than daylight images, because light scattering effects from dust on the front of the camera lens are greatly reduced (Malin *et al.*, 2017; Minitti *et al.*, 2019). Even though MARDI is slightly out of focus at ground level (its prime function was to serve as a landing descent camera), it still achieves *ca* 1 mm/pixel resolution over a 92 × 64 cm field of view aimed directly downward behind the left front wheel of the rover (e.g. Figure 2). The MARDI images used for this study were radiometrically corrected, geometrically linearized to compensate for lens distortion, colour balanced, and sharpened in Adobe Photoshop per the methods described in Minitti *et al.* (2019). Images examined for this study range from Sol 754 (i.e. the 754th Martian day of the MSL mission), when the rover entered the Murray Formation, to Sol 2,257, when the rover had largely completed exploration of Vera Rubin Ridge (VRR; Fraeman *et al.*, 2018). All images (a total of 2,025) were examined for abrasion features, regardless of lithology. Most of the directionally interpretable abrasion features were observed on mudstone surfaces, but a subset of the data was collected when the rover was driven across sandstone outcrops. The latter are identified in the maps that show the spatial distribution of wind directions as derived from abrasion features. The derived wind directions were plotted on base map images from the Mars Reconnaissance Orbiter High Resolution Imaging Science Experiment (HiRISE, McEwen *et al.*, 2007) that include an overlay of the rover traverse (Parker *et al.*, 2012; Calef and Parker, 2016).

2.3 | Data availability statement

Data presented in this paper are archived in the Planetary Data System (pds.nasa.gov).

2.4 | Nomenclature at the Gale Crater field site

Because there is no 'International Stratigraphic Code' for Mars, all the stratigraphic names (Figure 1) used in descriptions and figures are unofficial. With regard to geographic locations, the International Astronomical Union has only approved the names 'Gale', 'Aeolis Mons' and 'Aeolis Palus' (Figure 1), whereas other terms commonly used informally by the MSL team during flight operations are not (yet) officially approved.

2.5 | Laboratory experiments of Aeolian abrasion relevant to rover observations

On Earth, mudstones exposed to the surface environment are vulnerable to chemical and physical weathering by water, adverse influences with regard to the stable, long-duration surface exposure required for the development of well-formed aeolian abrasion features. Thus, on Earth aeolian abrasion features in mudstone outcrops are probably ephemeral phenomena and do not appear to have been discussed in the scientific literature. Due to this lack of known Earth analogs abrasion experiments have been conducted in the laboratory (Figure 4) in order to better understand the presumed aeolian abrasion features observed along the Curiosity traverse in Gale Crater (Figure 1). Abrasion experiments utilized: (a) a variety of mudstones, siltstones and evaporite (gypsum, anhydrite) rocks from geological formations in Indiana and Kentucky and (b) artificial samples where layers and features of contrasting hardness were produced with construction cement and plaster of Paris (gypsum). In several experiments the abrasion-induced mass loss of samples was monitored through the course of the experiment (Rossman *et al.*, 2012). Generally, the highest mass loss rates occurred in the initial weeks of a given experiment, followed by exponential decline as the exposed surfaces became increasingly 'streamlined'.

'Wind tails' and comparable features (Figures 1 and 2) are elongate, raised features, typically a few millimetres to centimetres wide and several centimetres to 10 cm or more in length. In many examples a more resistant element (e.g. an inclusion of sedimentary, volcanic or diagenetic origin) protrudes from the rock surface at the upwind end of the feature, and a 'tail' of less resistant rock material tapers downwind from this. Geometrically they resemble so called 'flutes' as described from sedimentary rocks on Earth (Reineck and Singh, 1980) and from ventifact studies (Bridges *et al.*, 2004; Laity and Bridges, 2009), but they are positive features on the surface, rather than scoop/spoon-like negative relief features. Whereas in many examples (Figure 1C) the erosion-resistant portion of the rock is a distinct feature (diagenetic nodule, sand grain or rock fragment; Schieber *et al.*, 2017), there are also examples where there is no readily apparent cause for tail formation (Figure 1D).

These features were reproduced in the laboratory by embedding small pebbles into blocks of gypsum (gypsum slurry poured into a rectangular mould) and exposing these samples to abrasion for periods of several weeks to as long as three months (Figure 5A). In addition, wind tails with more subtle relief formed on blocks of plain gypsum that were exposed to abrasion in the same experiments (Figure 5B). This indicates that minor, localized variations in cementation can yield sites of erosion resistance that are capable of developing wind tails.

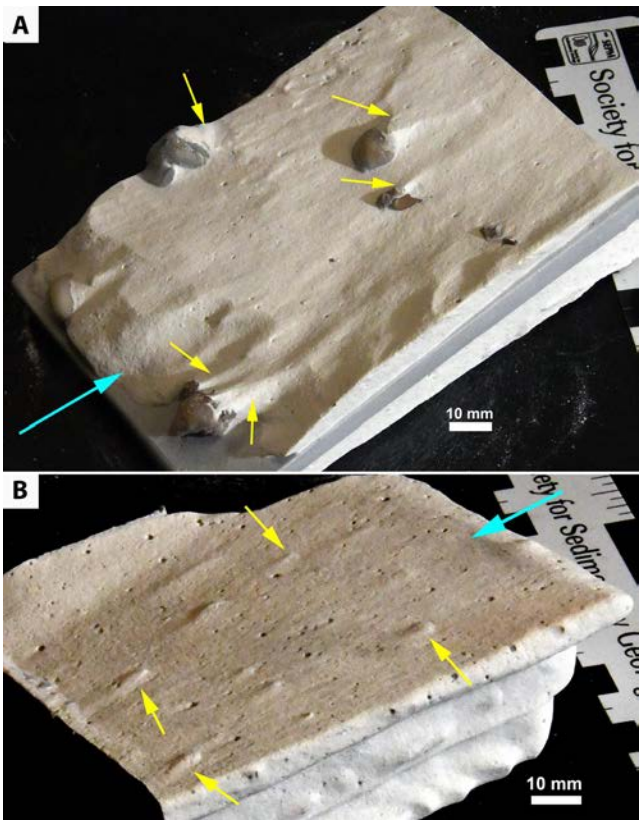

FIGURE 5 (A) Abrasion of gypsum block with embedded pebbles (dark, rounded features). Wind tails (yellow arrows) form in the erosion-protected region immediately downwind of the pebbles. Wind direction indicated by blue arrow. (B) Wind tail formation (yellow arrows) on block of pure gypsum. Wind direction indicated by blue arrow

In these experiments, flute-like (negative relief) features formed at receding block edges (Figure 6B), and along discontinuities of erosion resistance such as the contact between erosion-resistant silt layers and intervening softer mudstone layers (Figures 6D and 7). Analogous features can be observed in outcrops of the Murray Formation at the edges of fractured blocks of mudstone (Figure 8), or along fractures within large blocks (Figure 9).

In other experiments, siltstone layers, even those that were very thin, displayed more erosion resistance than intervening mudstone layers due to preferential cementation of silt layers. Wind erosion therefore drastically enhanced the relief and visibility of even very thin silt laminae (Figure 10). In addition to differential erosion, the resistant silt laminae developed short, remnant protuberances extending upwind, along with crenulated margins (Figure 9). Crenulated-serrated edges and remnant protuberances are also observed in MARDI images of the Murray Formation (Figure 11).

Another feature that was commonly observed in abrasion experiments is the formation of 'stalks' and 'pedestals'. These features develop due to differential erosion between diagenetic concretions with higher abrasion resistance than

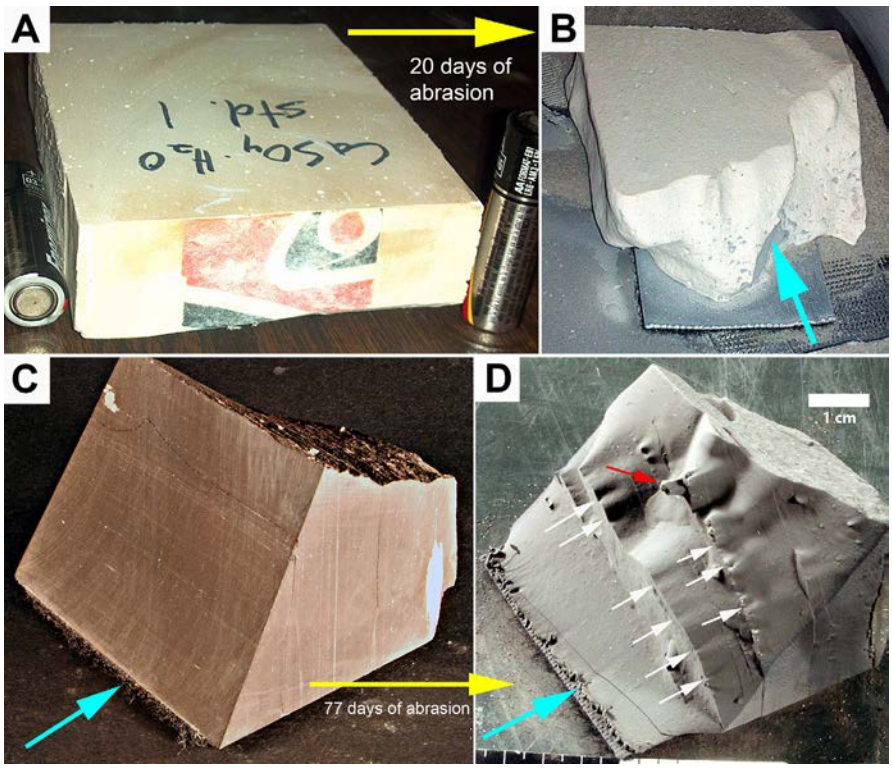

FIGURE 6 (A and B) experimental abrasion progress on a block of gypsum. Twenty days of abrasion have partially removed the upwind portion of the block (blue arrow = airflow direction) and generated a fluted edge. (C and D) experimental abrasion progress on a block of shale (layering is vertical; New Albany Shale, Indiana). Seventy-seven days of abrasion generated a stepped erosion profile that reflects alternating resistant silt layers and intervening softer mudstone layers (blue arrows = airflow direction). The silt-mudstone contacts show flute development (white arrows) in the mudstone layers. The red arrow points to a developing stalk

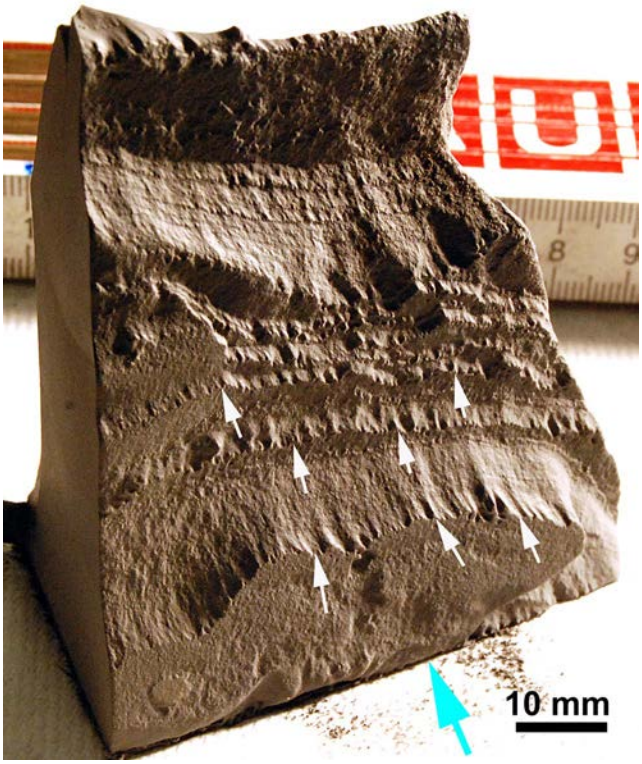

FIGURE 7 Another sample of shale (New Albany Shale, Indiana) with alternating silt (harder) and mudstone layers (softer). Layering is vertical. White arrows point to flute development in mudstone layers, downwind (blue arrows = airflow direction) of resistant siltstone layers

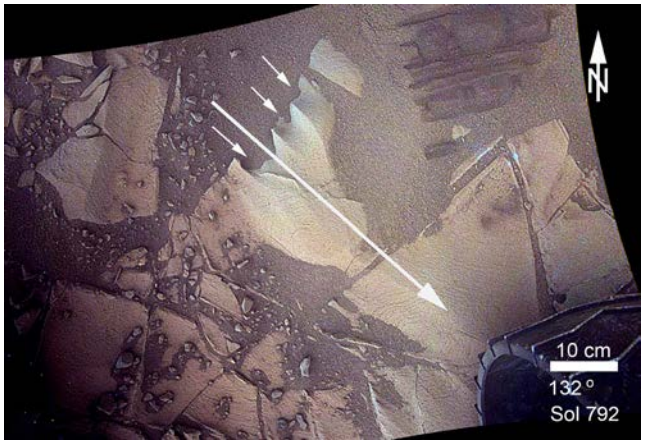

FIGURE 8 MARDI image of Murray mudstone shows formation of flutes at the edge of a block of bedrock (small white arrows). The prevailing wind direction that is deduced from this feature is indicated by the large white arrow. MARDI image 0792MD0003360000102998E01

the enclosing mudstone matrix. This phenomenon leads to clusters of 'pustules' projecting from the abraded surface (Figure 12), or to 'stalks' and 'pedestals' of matrix material that are protected from abrasion by resistant concretions at their tips. This phenomenon can result in remnant features projecting from sediment layers during erosional retreat (Figure 13) (cf. fig. 19.4 of Laity, 1994, and figs 19.12-19.13 of Laity, 2009). Morphologically similar features, termed

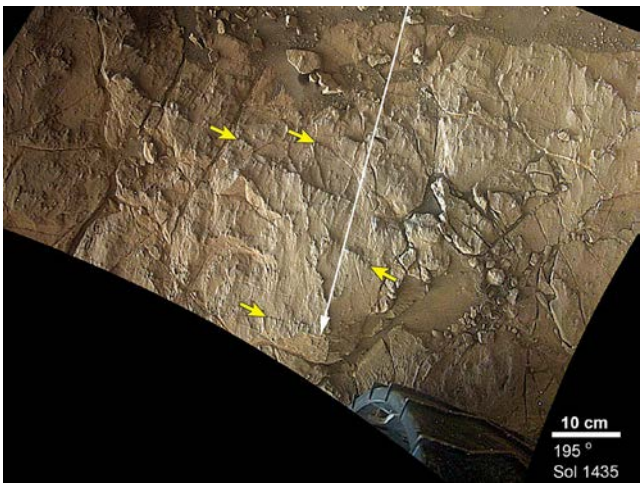

FIGURE 9 MARDI image of Murray mudstone. Yellow arrows point to low, fracture-related scarps where fluting has developed. The prevailing wind direction that is deduced from this feature is indicated by the large white arrow. Wind tails are apparent at upper right. MARDI image 1435MD0005430000200593E01

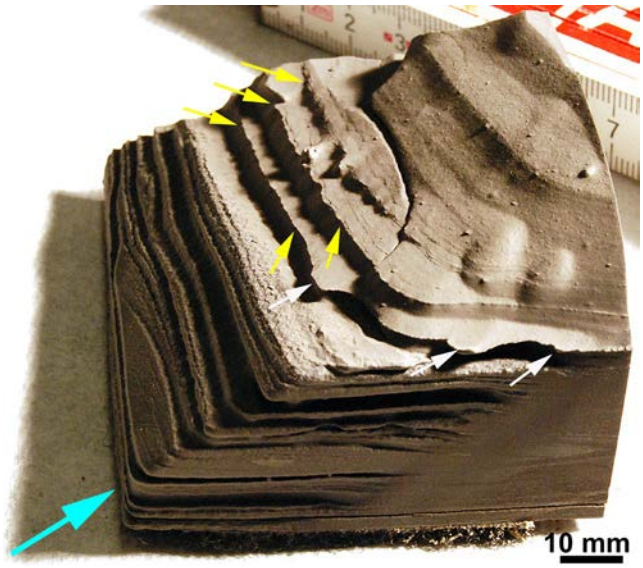

FIGURE 10 Experimentally abraded (30 days) interlaminated siltstone and mudstone (New Albany Shale, Indiana). In the lower half of the sample, mudstone intervals between siltstone form shadowed recesses. In the upper half (mudstone dominated), very thin silt laminae (sub-mm) resist erosion and stand out prominently. These resistant laminae (white and yellow arrows) show upwind promontories (white arrows) and edges that are crenulated. Blue arrow indicates airflow direction

'knobs and bosses', were described by Lancaster (1984) from the Namib desert, and are also known as 'dedos' (fingers in Spanish), as illustrated in Laity, 2011 (fig. 21.15). Comparable examples have also been illustrated from Meridiani Planum on Mars by Thomas *et al.* (2005).

More unusual and elaborate protruding features produced by aeolian abrasion have been imaged by the MSL rover cameras in multiple locations, with the most publicized example probably being that of the 'spoon' observed on Sol 1,090 of the MSL mission (Figure 14). The great majority of stalk and pedestal features are smaller and less spectacular, but nonetheless are widespread and are apparent in many MSL outcrop images (Figure 15).

On Earth, differential erosion of sedimentary strata enhances surface relief of more resistant layers, helping draw attention to what otherwise might be relatively subtle differences caused by ancient environmental or depositional changes. In the experiments described here, aeolian abrasion of mudstones and gypsum analogs resulted in enhanced relief according to layer-by-layer differences in erosional resistance (Figures 16 and 17; preferential removal of softer mudstone layers is also visible in Figures 10 and 13). On Mars, the downward view from MARDI typically is more at right angles to sedimentary bedding planes exposed at the surface, rather than parallel to them, so differential erosion is not as apparent in MARDI images as in Figures 10 and 13. However, other rover cameras have recorded many examples of Martian sedimentary rocks expressing this style of differential erosion (e.g. Figure 18).

2.6 | Surface variability of airflow—past and present

Although in most instances the airflow direction indicated by aeolian abrasion features is reasonably uniform across the MARDI field of view (Figures 2, 9 and 15), some images show more complex patterns that reflect local interactions between surface topography and airflow that have affected abrading sand trajectory azimuths (Figure 19). Other examples of short range surface flow variability are shown in Figures 20 and 21. The latter two images also show how wind directions derived from abrasion features compare with modern wind directions deduced from wind ripples and sand accumulations behind obstacles.

2.7 | Mapping wind patterns

Systematic inspection of MARDI images acquired from Sol 754 to 2,257 of the MSL mission yielded 229 sand abrasion directions, derived from aeolian abrasion features similar to examples in Figures 1, 2, 5 through 13, 15, 19, 20 and 21. In addition, 30 modern wind directions were determined from sand accumulation behind obstacles (e.g. Figure 19) and wind ripples in sand (e.g. Figures 20 and 21). Arrows indicating wind directions were plotted on a composite of orbital HiRISE images (Figures 22 through 28) that serve as

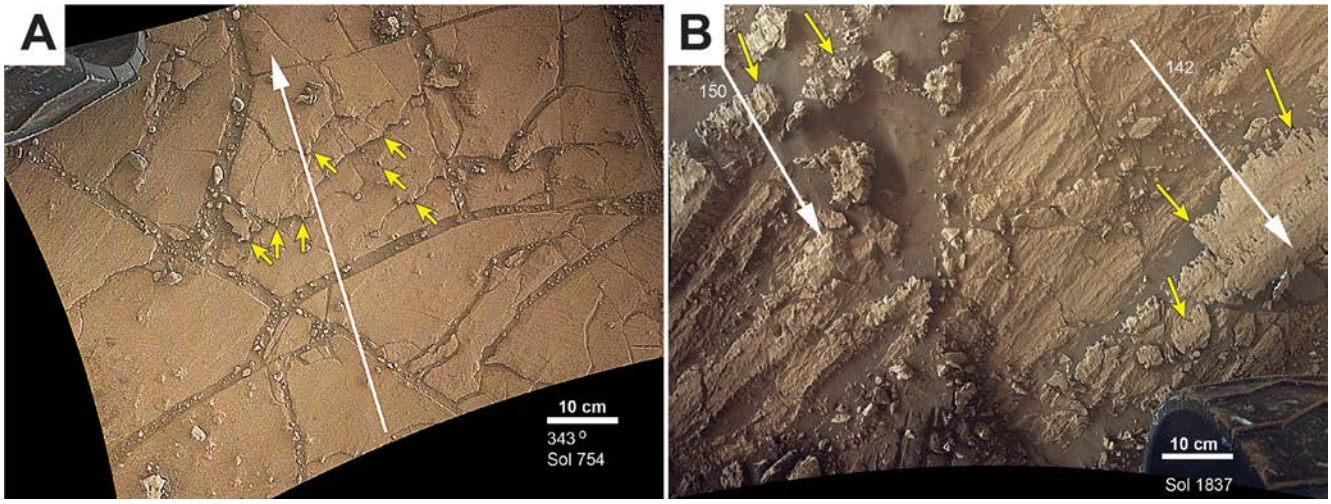

FIGURE 11 MARDI images that show features comparable to Figure 10 in the Murray Formation. (A) Resistant laminae with promontories (yellow arrows), interpreted as aeolian abrasion remnants that project upwind. The white arrow marks the interpreted direction of airflow. MARDI image 0754MD0003260000102475E01. (B) Crenulated-serrated edges of resistant laminae (yellow arrows) that are interpreted to record the effects of abrading sand that was blowing from the upper left to the lower right (large white arrows). MARDI image 1837MD0007470000200793E01

a basemap for the MSL mission (Parker *et al.*, 2012; Calef and Parker, 2016). The data density is not uniform because (a) drive distances between MARDI image locations varied along the traverse and (b) some traverse segments ended with the rover paused over ground with abundant sand and rubble, instead of outcrop.

The first of these maps (area A, shown in Figure 23) shows the rover traverse southwest from the Pahrump Hills outcrops. In general, rock abrasion directions in Figure 23 record sand mobilized to the south-southeast. A southeast direction (135°) dominates at Pahrump Hills. In the vicinity of the sol 971 rover position, rock abrasion directions are consistent with topographic modification of wind-driven sand pathways around a hill. Modern sand deposits (commonly in depressions) exhibit large ripples with a range of orientations, suggesting multiple sand transport directions across area A that probably reflect topographic control of near-surface airflow and sand pathways in this highly dissected terrain.

Figures 23 and 24 show that rock abrasion directed south-southeast characterizes many mudstone surfaces in areas A and B. Confusing exceptions exist in area B (Figure 23) near the sol 1,100 rover position where intricate surface relief provides opportunities for many diversions and blockings of sand migration pathways. Within area B, which includes a portion of the Bagnold dune field (see Bridges and Ehlmann, 2017), there is an abrasion subset directed west to southwest that spans the *ca* 100 m corridor between Namib dune and High dune, as if caused by sand blowing from one dune across to the other. In this hypothesis sand supply azimuth would be a decisive factor (in addition to wind azimuth), as discussed earlier. In an analysis of HiRISE images of nearby dunes, Silvestro *et al.* (2013) proposed two formative regional wind directions, blowing west-southwest and southeast, in order to explain ripple orientations of 330° and 45° on nearby dunes (with the caveat that Martian ripples large enough to be resolved from orbit do not always reflect transverse wind directions across their crests; Silvestro *et al.*, 2016). Accordingly, net south-southwest sand transport directions for High dune and Namib dune, estimated from their slipface orientations (larger green arrows in Figure 24) could reflect contributions from both of these proposed regional formative winds. In the corridor between Namib dune and High dune, sand saltating west-southwest dominates the abrasion textures (over the southeast or south-southeast textures found elsewhere) because of the abundant local sand supply adjacent to the corridor and immediately upwind of it (i.e. to the east-northeast of it) represented by Namib dune. In this interpretation, sand blowing from Namib dune when winds blow to the west-southwest dominates abrasion textures in the rock corridor immediately downwind, overwhelming any signatures there of sand-limited abrasion from regional winds blowing south-southeast that prevails elsewhere in area B.

In Figure 25, a striking feature in area C is the northeast abrasion directions dominating one area of the Naukluft Plateau (blue arrows). These directions were measured in sandstone outcrops of the Stimson Formation, a unit that unconformably overlies the Murray Formation (Banham *et al.*, 2018). Although this study is focused on the Murray Formation, observations from the Stimson are included here because they form part of the rover traverse and allow for added perspective on ancient wind patterns. Due to the generally higher erosion resistance of the sandstones, oriented aeolian abrasion features are less common and not as well developed as in mudstones along the MSL traverse. In addition, aeolian abrasion in sandstones may not be directly comparable to that seen in mudstone outcrops. Whereas in mudstones an included hard grain or a concretion tends to lead to well-developed 'wind tails', in a sandstone the contrast in

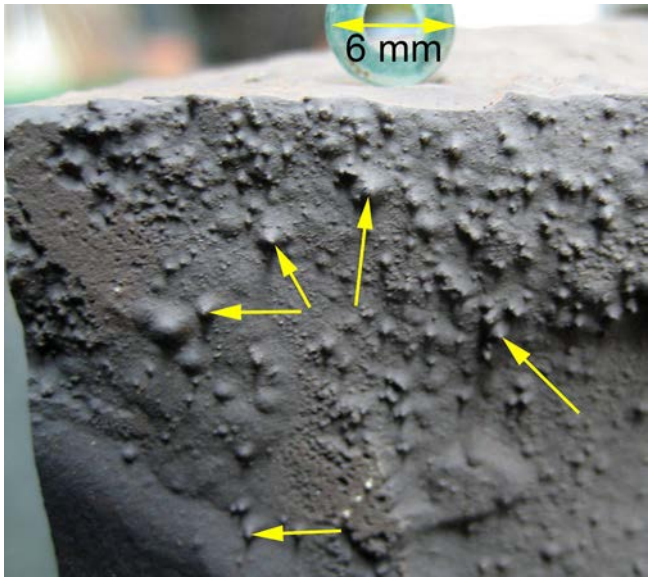

FIGURE 12 Abraded shale specimen (New Albany Shale, Indiana) with 'pustules' (yellow arrows). In this sample bedding was perpendicular to the particle/airflow. Abrasion was retarded by numerous sub-millimetre pyrite concretions that consequently became elevated on a pedestal of matrix mudstone

resistance between a pebble or a concretion and the surrounding sand grains (also hard) is probably less pronounced and as such wind tails are less well-developed. In a poorly cemented sandstone, however, differential abrasion should be better developed and 'wind tails' should develop more readily. On this basis, abrasion directions derived from sandstones can be expected to be more irregularly distributed and to carry a higher uncertainty than those measured on mudstone surfaces. On the other hand, the overall coherence of northeast abrasion directions measured on the Naukluft Plateau just east of the Sol 1,357 rover site (Figure 25) suggests that this orientation is significant. Possibly the greater erosional resistance of this sandstone surface (probably partly responsible for its expression as a plateau, standing higher than surrounding terrain) represents a more ancient exposed surface than less resistant mudstones elsewhere along the rover traverse, and might record abrasion textures from a previous epoch where sand pathways were different from the present day. In support of this hypothesis, abrasion directions derived from mudstone outcrops in area C are generally similar to overall southerly transport pathways observed earlier in the traverse (areas A and B, Figures 23 and 24). Also, within area C present-day sand migration is westward, as indicated by the large ripples in modern sand deposits (assuming that sand pathways are transverse to these large ripple crests), further suggesting a different, older origin of the northeast abrasion orientations.

The clustering of northeast abrasion directions in sandstones from the Naukluft Plateau (Figure 25) may thus represent a combination of (a) an abrasion signature of older wind directions that has since been obliterated from the softer and more readily abraded Murray mudstones, (b) a higher density of rover stops (closely spaced MARDI images), and (c) locally softer Stimson sandstone that allowed for better development of 'wind tails' more recently.

In area D (Figure 26), the rover travelled over a gently sloping mudstone surface through the Murray Buttes and beyond. Abrasion directions measured in this area show limited scatter and indicate rock abrasion from saltating sand migrating to the south-southeast. The southerly course of the rover through area D avoided close approaches to the buttes and areas that might have been screened by individual buttes from sand migrating southward. However, the sol 1,455 rover position was an exception. There, the rover ventured westward a short distance 'behind' one of the buttes (i.e. southward surface pathways would be blocked by the butte itself). Abrasion textures at this location are west-southwest, either reflecting wind and sand pathways that were deflected around the butte, or perhaps reflecting the abrasion signature of a secondary sand-driving wind azimuth common in the region but revealed only in this location where a more dominant, regional south-southeast abrasion signature cannot reach and obliterate it. Unfortunately, comparisons of rock abrasion measurements with modern sand migration directions in area D are complicated by the general lack of extensive modern sand deposits: Many of the most prominent ripple crests in orbital views are light-toned, consistent with a dust component indicating inactivity and probably induration. Darker sand deposits in the region occur mostly only as mantles covering steep debris aprons surrounding individual buttes, and thus are unsuitable for assessing current regional sand migration pathways.

Southerly sand abrasion textures continue as the rover traverse extends into area E (Figure 27), until encountering the Bagnold dune field for the second time around Sol 1,600. While traversing the corridor between Mount Desert Island dune and Nathan Bridges dune, abrasion directions are more irregular but include sand pathways to the southwest, the current migration direction of linear ripples and dunes encountered by the rover and observed nearby from orbit (Silvestro *et al.*, 2016; Lapotre and Rampe, 2018). These southwest-pointing abrasion textures become more consistent as the rover traverse continues among numerous outlying ripple fields of mafic sand while emerging from the dune field. In this region (southern portion of area E) abrasion textures are similar to modern sand migration directions suggested by crest orientations of large ripples resolved from orbit (with the caveat mentioned earlier that actual sand motion might not be orthogonal to these ripple crests; Silvestro *et al.*, 2016). The rover traverse continued across mudstones as it approached the higher standing VRR (Figure 22), which barely extends into area E as a

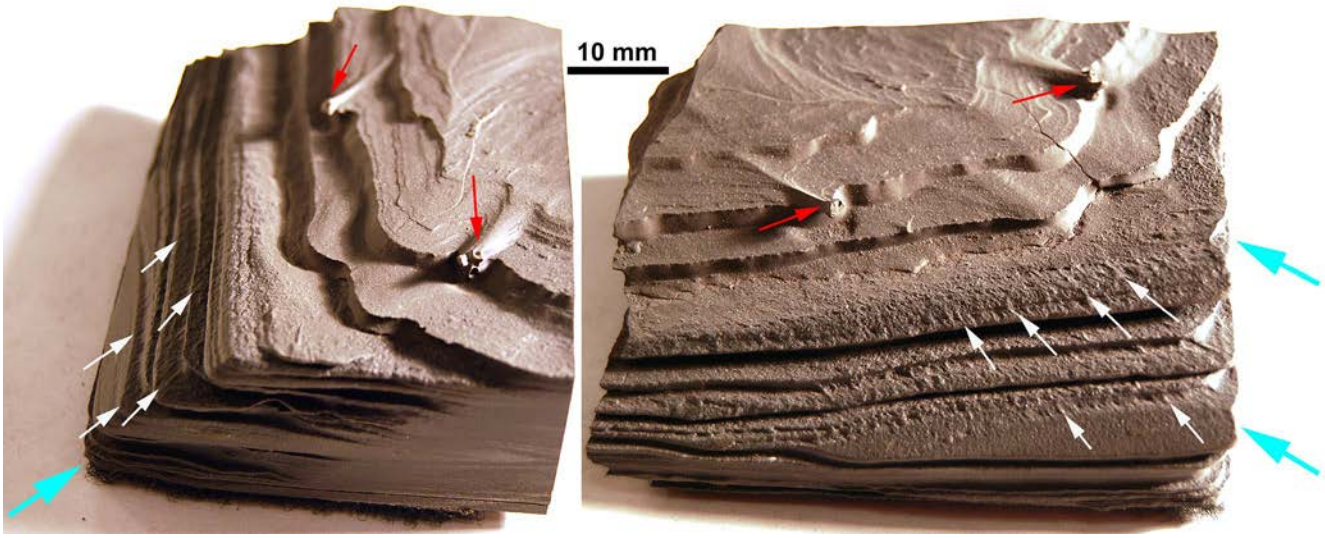

FIGURE 13 Sample of interlaminated siltstone/mudstone (lower 2/3 of sample) and recessive mudstone (upper 1/3 of sample). Sample (New Albany Shale, Indiana) shown from two perspectives, airflow direction shown by blue arrows. Red arrows point to mudstone stalks/pedestals that are protected from erosion by resistant pyrite concretions. This sample is the same as pictured in Figure 10, but 84 days later in the same abrasion experiment (114 days total experiment time). In Figure 10, the stalks/pedestals had just started to develop. In the laminated siltstone portion (lower 2/3 of the specimen), erosional striations have developed (white arrows), that over time may develop into serrated lamina edges like those seen in Figure 11B

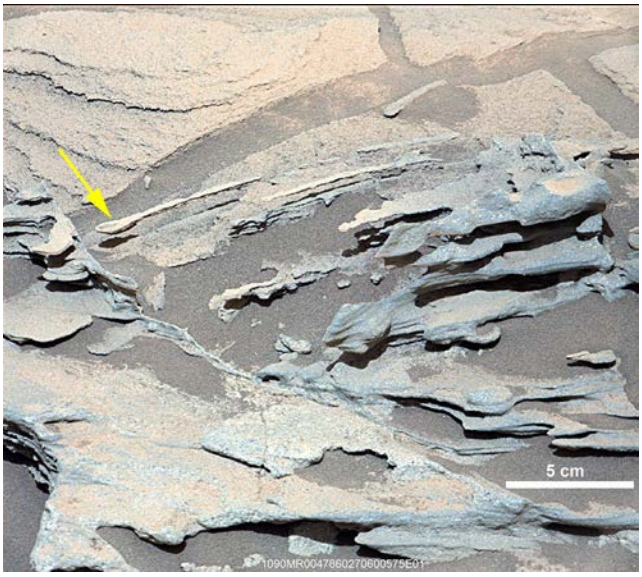

FIGURE 14 The 'spoon' (yellow arrow), a handle shaped feature that juts out from an outcrop and ends in a rounded tip. The rock is a sandstone in this case, but the 'spoon' does look very delicate and attests to the very gentle yet persistent action of aeolian abrasion on the surface of Mars. Mastcam image 1090MR0047860270600575E01

light-toned mass at the extreme lower right of Figure 27. Just as the strata below it, the VRR consists largely of mudstones. It appears to be more erosion resistant and forms an escarpment (Figure 28), a circumstance that is attributed to better cementation of these rocks (Fraeman *et al.*, 2013; Fraeman *et al.*, 2018; Bennett *et al.*, 2018; Rivera-Hernandez *et al*., 2019). In this area, abrasion orientations on mudstones appear to deflect around the steeper slopes of the VRR.

Abrasion directions on the VRR (area F, Figure 28) are southerly overall, but northern portions of the ridge exhibit abrasion from sand moving southeast, whereas southern portions of the ridge display mostly southwest abrasion. Large modern sand deposits on the ridge are rare, providing little access to present-day sand migration directions for comparison with rock abrasion orientations. However, within an irregular sand patch near the Sol 2,163 position, narrow sand 'tails' extending from individual rocks (essentially small directed drifts similar to 'sand shadows' discussed by Bagnold (1941), indicate sand currently moving west-southwest at that location.

The rover explored the VRR for 500 sols, but Figure 28 shows that in many rover locations no directional data could be recovered. The reason for this is not so much an absence of aeolian abrasion features, but rather an abundance of ambiguity (Figure 29). As already indicated above, the mudstones of the VRR form an escarpment, owing to an erosion resistance (Fraeman *et al.*, 2013, 2018; Bennett *et al.*, 2018; Rivera-Hernandez *et al*., 2019) that is substantially greater than that of typical Murray Formation mudstones encountered between Sols 754 (base of Murray) and 1,800 (base of VRR). The more resistant rocks of the VRR commonly record aeolian abrasion from different wind directions on separate facets (Figure 29), not unlike what is observed in ventifacts.

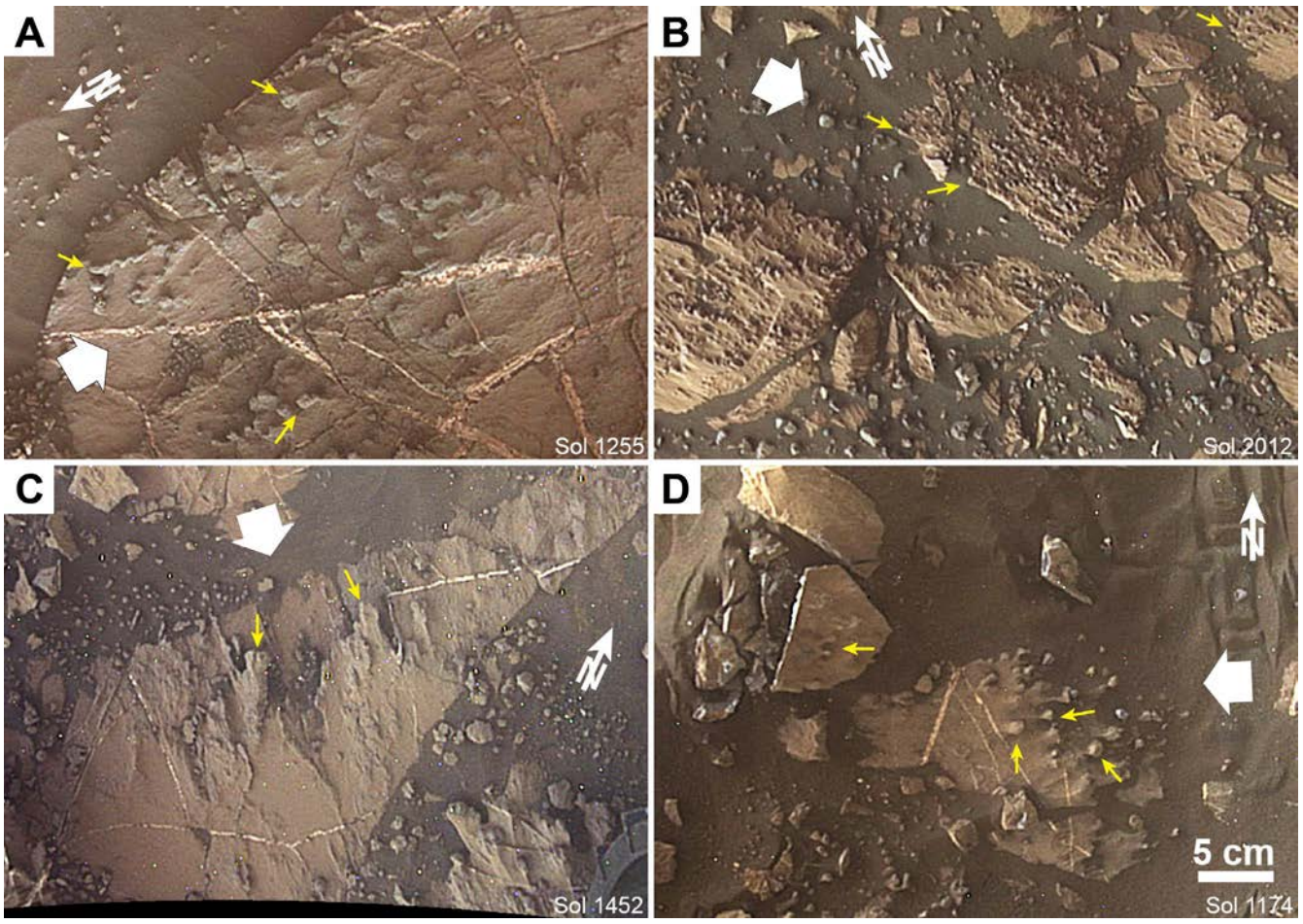

FIGURE 15 Examples of MARDI images that show protruding stalks and pedestals similar to those formed in abrasion experiments (Figures 12 and 13). These features can be somewhat bulbous and thickened upwind, suggesting that rounded concretions or inclusions of greater abrasion resistance are the underlying cause (images A, B and D). Planar or flat projections suggest erosional enhancement of layers with somewhat greater erosional resistance (image C). In each image, white arrows suggest the overall sand saltation direction indicated by orientations of stalks and pedestals (yellow arrows). MARDI images (A) 1255MD0004690000200407E04, (B) 2012MD0007940000201049E01, (C) 1452MD0005490000200599E01 and (D) 1174MD0004450000200001E01

3 | DISCUSSION

Laboratory experiments described in previous sections illustrate how aeolian abrasion against windward rock surfaces can develop features such as flutes, grooves, wind tails, pedestals and stalks, and enhance the surface expression of more resistant laminae through differential erosion. The experiments clearly show that these features are consistent with unidirectional particle trajectories impacting target surfaces, and confirm many prior studies that the direction of sand motion can be deduced from their morphology. Features of this kind were produced in previous experiments (Bridges *et al.*, 2004; Laity and Bridges, 2009) utilizing a range of rock types and rock simulants, but prior studies where mudstones were subjected to aeolian abrasion experiments are lacking. Laity and Bridges (2009) concluded that sand was the most probably abradant to form such features (on Earth and Mars), that sand abrasion and ventifact formation occur only on the windward side of a target, and that characteristic abrasion features such as flutes, grooves and pits develop best where target surfaces are exposed to sand saltation from a consistent direction, reinforcing conclusions of earlier studies that ventifacts and abraded terrain can allow derivation of sand-driving palaeowind patterns (Sharp, 1949).

In these experiments, stalk and pedestal formation (Figures 11 and 12) occurred only when sand trajectories were unidirectional for a significant experiment duration (2–3 months' continuous saltation exposure, in the case of mudstone samples). Because these features develop where a resistant object, such as a concretion, protects the softer mudstone matrix downwind from erosion, the 'softer' pedestal is eroded away and stalks disappear if samples are intermittently rotated. Therefore, instances of stalks and pedestals developed in Murray Formation mudstones signify where sand saltation from a consistent direction has occurred over long time periods. In Gale Crater, saltation directions derived

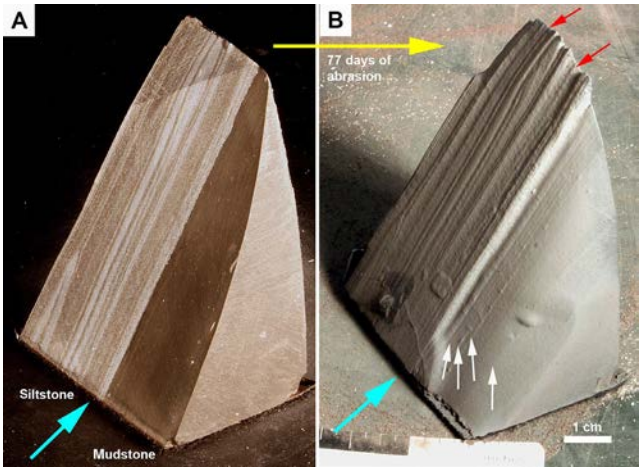

FIGURE 16 Experimental abrasion of a mudstone sample (New Albany Shale, Indiana) that consists of cemented siltstone layers and mudstone layers. At left (A) the sample prior to abrasion, and at right (B) the same sample after 77 days of continued abrasion. Whereas in (A) the initial saw-cut surface was continuous across both siltstone and mudstone portions, after prolonged abrasion (B) the mudstone portion has retreated and has a smoother appearance than the siltstone portion. Erosion has brought out faint laminae in the mudstone (white arrows). The most resistant siltstone layers (light coloured in (A) developed in positive relief during the experiment (B). Darker and more muddy interlayers were gouged out (red arrows) by abrasion

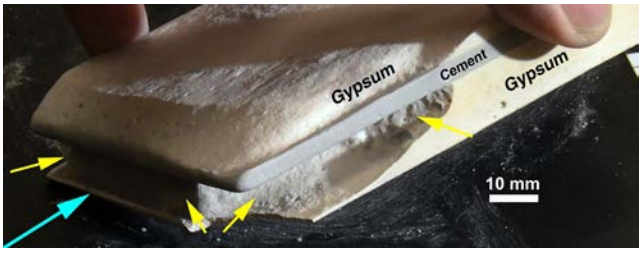

FIGURE 17 Experimental analogue sample that shows differential erosion between gypsum and cement layers. Sharp undercutting of soft gypsum (yellow arrows) contrasts with more resistant cement layer that starts to project out in positive relief. Sand abrasion direction (airflow direction) shown by blue arrow

from multiple locations reveal relatively coherent wind patterns within a given area (Figures 22 through 27), and this supports the motivating premise of this study, intending to document regional, and in places local, sand-driving wind patterns.

Overall wind directions indicated by wind tails and associated abrasion features within the Murray Formation are towards the south and south-southeast along the Sol 754 to 2,257 rover traverse (Figure 22), although for smaller sampling areas the influence of topography becomes more readily apparent. For example, in Figure 23, abrasion directions for the smoothly sloping area of the Pahrump Hills outcrop are similar, but as the rover advanced to the

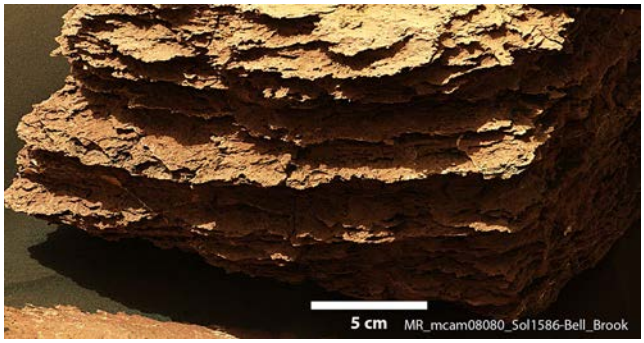

FIGURE 18 Preferential removal of softer mudstone intervals in a block of wind eroded Murray Formation mudstone, as seen during the rover's ascent of Mount Sharp. Here the Murray contains abundant, approximately bedding-parallel fractures, filled with calcium sulphates, that are more abrasion resistant than the mudstone that encloses them. Consequently, the mudstone portions of this rock are deeply recessed, and most of what is seen in this image are the calcium sulphate vein fills. Image mosaic composed of Mastcam images 1586MR0080800010800381E01 and 1586MR0080800020800382E01

southwest into more dissected terrain, more directional scatter is apparent, as well as deflection of wind flow and sand pathways around elevated topographic features (near the Sol 971 marker).

The Curiosity rover carries the Rover Environmental Monitoring Station (REMS) wind sensor (Gómez-Elvira *et al.*, 2012) which operated until *ca* Sol 1,500. Although the measurements show complex wind patterns and great variability related to time of day and season, local scale circulation appears to dominate observed surface winds in Gale Crater (Viúdez-Moreiras *et al.*, 2019a; 2019b). Although one might wonder whether this complexity might lend itself to wind sculpted rocks that show multiple transport directions, because in experiments directional abrasion features became apparent within a few weeks it is highly probably that surfaces that might carry multidirectional wind tails are a transient phenomenon at best. Wind measurements with the REMS sensor suggest peak wind speeds for upslope winds (towards the south) during the southern hemisphere summer (Viúdez-Moreiras *et al.*, 2019a, 2019b). Thus wind directions derived from abrasion features are broadly consistent with observed wind directions from REMS. The south-facing slip faces of Namib and High dune (Figure 24, heavy blue arrows) are also consistent with winds from the north that push sand in an upslope (to the south) direction, and suggest that a slope wind regime appears to impact modern sand movement and may well be an underlying cause for the regionally observed southward orientation of wind tails and associated abrasion features that formed over longer time scales.

In Figure 24, the terrain flattens and the dominant south-southeast direction is again well-developed. In the Bagnold 1 area, however, in the gap between Namib and High

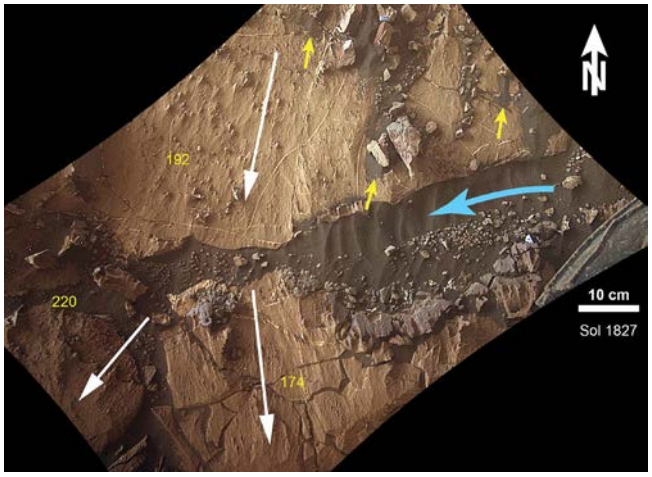

FIGURE 19 Three different sand abrasion directions (airflow directions) in a single MARDI image are shown by white arrows (azimuths indicated with yellow lettering). Abrading sand generally moved southward, but locally flow seems to have been affected and modified by more resistant obstacles and debris-filled fractures. In part, modern sand transport (and thus abrasion) directions coincide with southward directions indicated by abrasion features, for example as indicated by sand tails behind surface obstacles (yellow arrows). Yet, in other places they show considerable divergence. For example, the blue arrow shows wind-ripple crests that suggest roughly east-west ripple migration (airflow) in a sand-filled fracture, an indication that modern transport orientations can be substantially more complex than those we see recorded by abrasion features that are biased towards long-term prevailing winds. MARDI image 1827MD0007410000200787E01

FIGURE 20 Comparison of wind directions as recorded by abrasion features in mudstone (white arrows) with modern wind directions as recorded by rippled sand (blue arrow). Whereas abrasion features indicate a dominant southerly airflow, the modern sand ripples show how surface airflow and low-angle saltation grain trajectories tend to follow sand-filled depressions around obstacles. MARDI image 1473MD0005600000200610E01

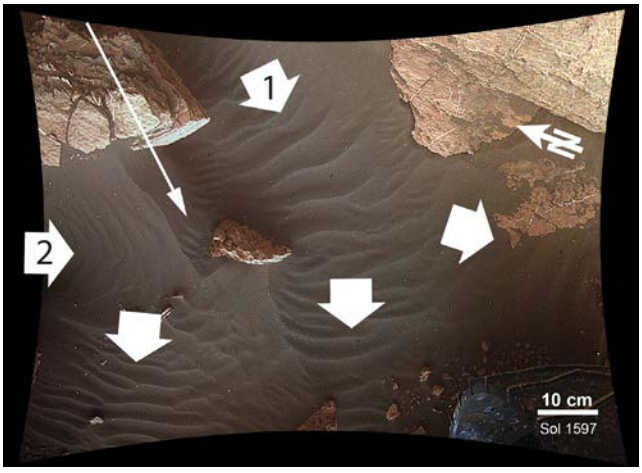

FIGURE 21 Comparison between airflow derived from abrasion features (SSE pointing narrow white arrow), and airflow indicated by modern ripples in loose sand (wide white arrows). Modern sand transport directions are similar to the long-term SSE abrasion direction (arrow 1). Yet, low-angle saltating grain trajectories of modern sand deposits in local low areas are influenced by higher standing rocky obstacles, resulting in some variation in azimuths of access (e.g. arrow 2). MARDI image 1597MD0006120000200662E01

dune, abrasion from sand saltating west and southwest indicates that azimuth of sand availability is an essential factor when evaluating the development history of aeolian abrasion features. The barchan dunes in Figure 24 have slip faces that indicate migration to the south-southwest (green arrows) and superimposed smaller ripples that are migrating west-southwest (yellow arrows). The Bagnold Dunes, and the sand that forms them, broadly migrate to the southwest (Figure 22), and thus the sand flux in bedrock areas between dunes should be higher than in bedrock areas that are not in the path of dune migration. Given that migration of the modern dunes reflects the modern wind regime, the west and southwest abrasion directions recorded locally between dunes probably reflect the influence of nearby dune sand sources and relatively frequent saltation events from these sources. The south-southeast abrasion directions recorded on bedrock surfaces outside the dune migration path probably record long-term sand saltation at much lower rates (e.g. from rare strong wind events, but consistently from the north-northwest) that mobilize more diffuse sand sources somewhere upwind to the north-northwest, perhaps even ultimately from outside Gale Crater. In this concept, south-southeast sand migration potentially has affected and continues to affect bedrock surface textures across much of this part of the Gale Crater floor, but is overwhelmed in local areas between dunes by more active saltation abrasion along the dune migration path. Some support for this idea is provided by the orbital analysis of Silvestro *et al.* (2013), which discussed how secondary wind currently blowing from northwest to southeast would be consistent with a distinct subset of ripple orientations they measured on the Bagnold Dunes.

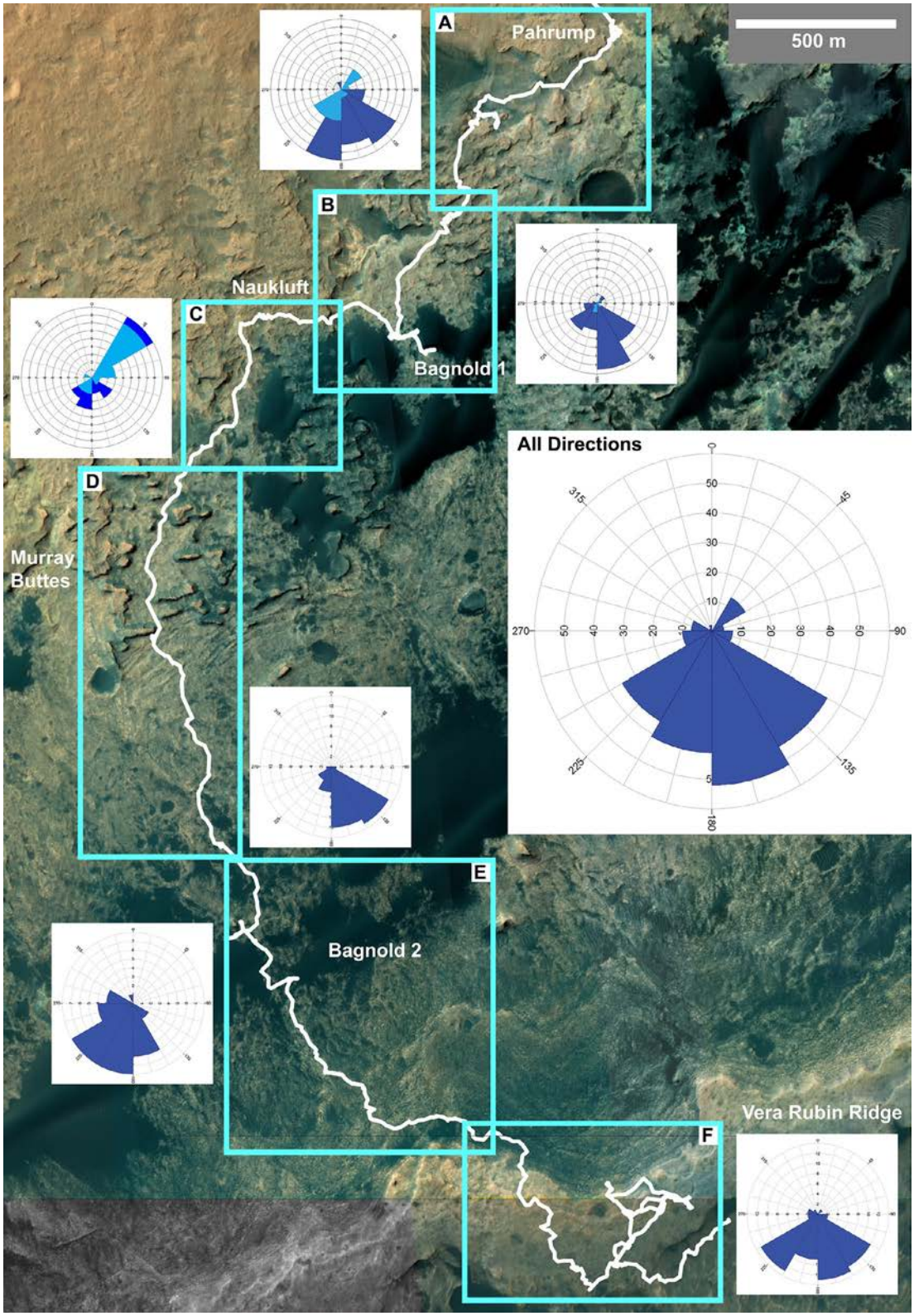

FIGURE 22 HiRISE image composite of the northern foothills region of Mount Sharp with the rover path indicated by the white trace. The wind direction arrows are difficult to plot legibly at this level of magnification, and are instead displayed on six (labelled A through F) enlarged detail maps (Figures 23 through 28). The location and coverage of each detail map is indicated by six blue rectangles. The large rose diagram at right (all directions) shows the distribution of wind directions from the entire traverse (229 directions). The smaller rose diagrams next to each detail region show the distribution of derived wind directions for detail regions. They are shown in more detail in Figures 23 through 28. As the rover progressed from area (A–F) it generally moved uphill to successively higher elevations

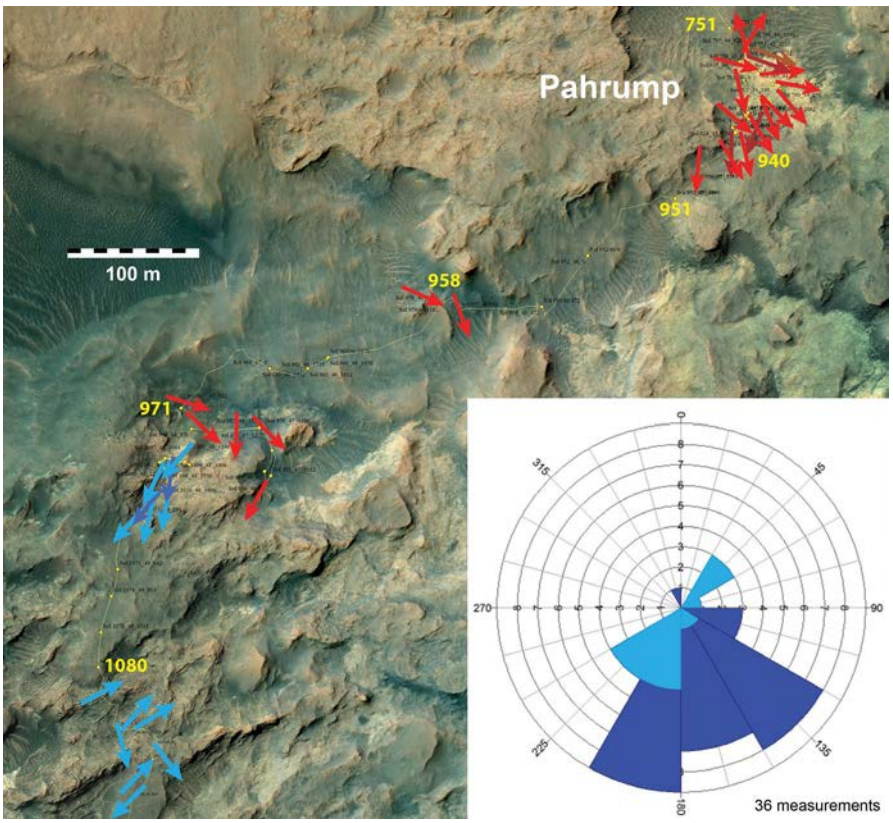

FIGURE 23 Region 'A' from Figure 22. Red arrows show wind directions derived from aeolian abrasion features in MARDI images of mudstone exposures. Blue arrows show wind directions collected from sandstone exposures. In areas where arrows are crowded together, some arrows were given a different shade of red to aid visibility. The rose diagram shows the distribution of wind directions (dark blue from mudstones, light blue from sandstones), and the numbers in yellow provide guidance on the time (Sol) the rover traversed these locations

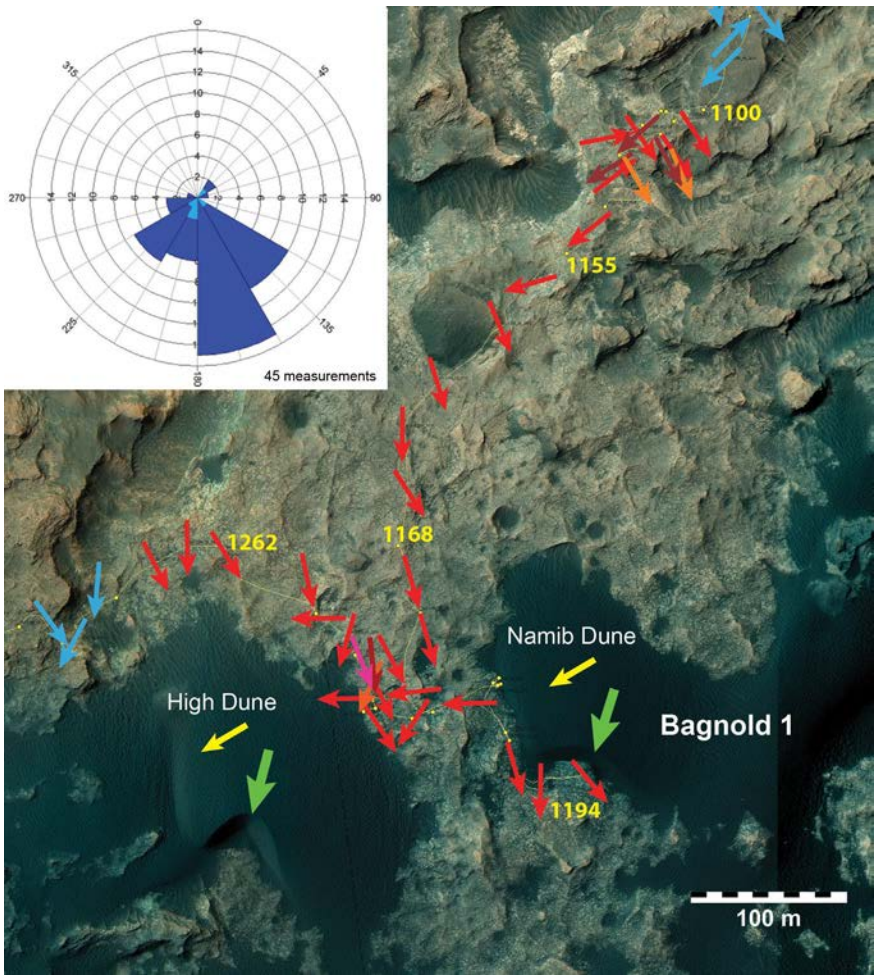

FIGURE 24 Region 'B' from Figure 22. Red arrows show wind directions derived from aeolian abrasion features in MARDI images of mudstone exposures. Small blue arrows show wind directions collected from sandstone exposures. In areas where arrows are crowded together, some arrows were given different shades of red to aid visibility. Dark areas are covered with actively moving sand dunes (Bagnold Dunes, investigation area 1). The identifiers "High dune" and "Namib dune" are from Bridges and Ehlmann (2017). The arrows on the dunes indicate the slip face propagation direction (SSW, 195°, large green arrows), and the migration direction of superimposed metre-scale ripples (SW, 235°, yellow arrows). The rose diagram shows the distribution of wind directions (dark blue from mudstones, light blue from sandstones), and the numbers in yellow provide guidance on the time (Sol) the rover traversed these locations

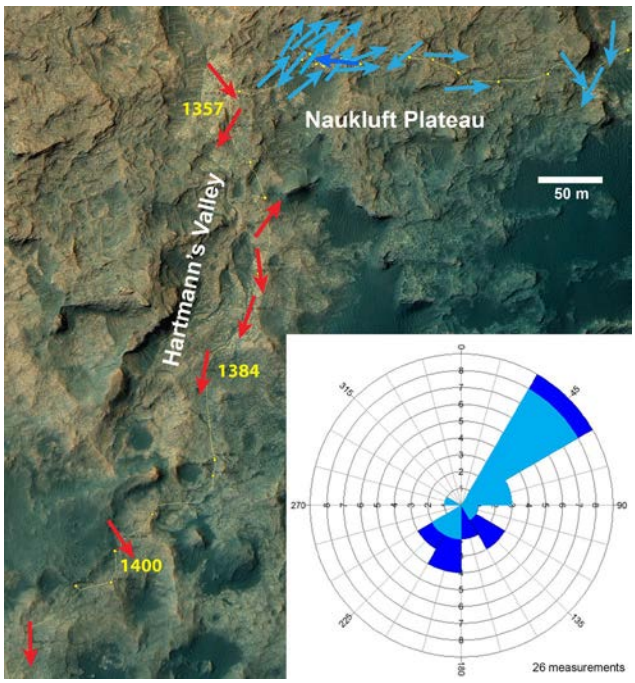

FIGURE 25 Region 'C' from Figure 22. Shows wind directions derived from aeolian abrasion features in MARDI images. Red arrows indicate abrasion features in mudstones. Blue arrows indicate abrasion features in Stimson sandstone of the Naukluft Plateau area. The rose diagram shows the distribution of wind directions (dark blue from mudstones, light blue from sandstones), and the numbers in yellow provide guidance on the time (Sol) the rover traversed these locations

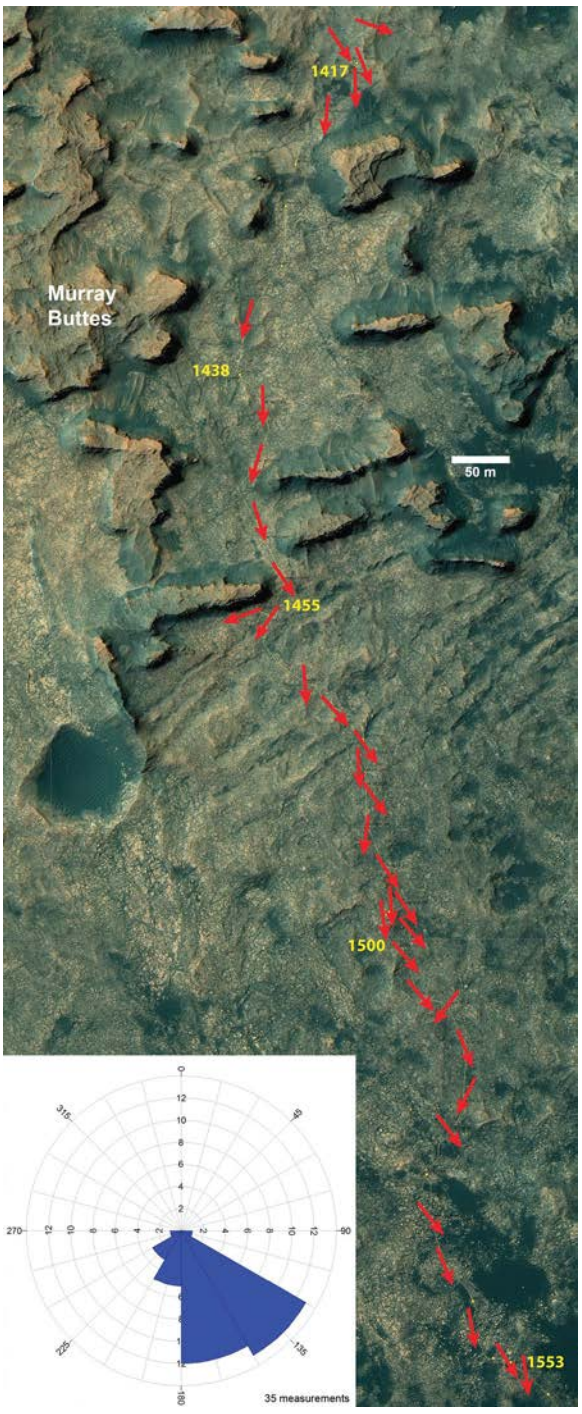

FIGURE 26 Region 'D' from Figure 22. Red arrows show wind directions derived from aeolian abrasion features in MARDI images of mudstones. The rose diagram shows the distribution of wind directions, and the numbers in yellow provide guidance on the time (Sol) the rover traversed these locations

Abrasion directions indicating west to southwest sand saltation are also dominant along the MSL traverse at Bagnold 2 and in areas immediately to the south, where the traverse is adjacent to numerous sizeable, probably active, sand deposits (Figure 27). This observation supports the premise that modern sand movement is responsible for aeolian abrasion features in these areas. Further south and more distant from the Bagnold Dunes, southeast abrasion directions dominate the long stretch of Murray bedrock exposure (largely mudstone) along the MSL traverse from Sol 1,417 to 1,553. Along that part of the traverse only minor sand patches occur, mainly in depressions (Figure 26). These southeast abrasion measurements could indicate effects from less common sand-driving wind events towards the southeast (consistent with the suggestion of Silvestro *et al.* (2013) that secondary winds from the northwest currently influence ripple orientations on the Bagnold Dunes) which would mobilize sand from sources to the northwest of this area, including from the Bagnold Dunes.

The wind directions recorded from the Stimson sandstone outcrops of the Naukluft Plateau (Figure 25) constitute the most outstanding deviation from the otherwise dominant southerly abrasion directions (Figure 22). Given that sandstones and siltstones tend to be much more erosion-resistant in abrasion experiments than mudstones (Howald and Schieber, 2008; Rossman *et al.*, 2012), it is probably that 're-orienting' aeolian abrasion features in sandstones also requires substantially longer time intervals than for comparable features in mudstones. As such, abrasion directions recorded on the Naukluft Plateau may represent an older wind regime. That this is a distinct possibility is suggested by Bridges *et al.*

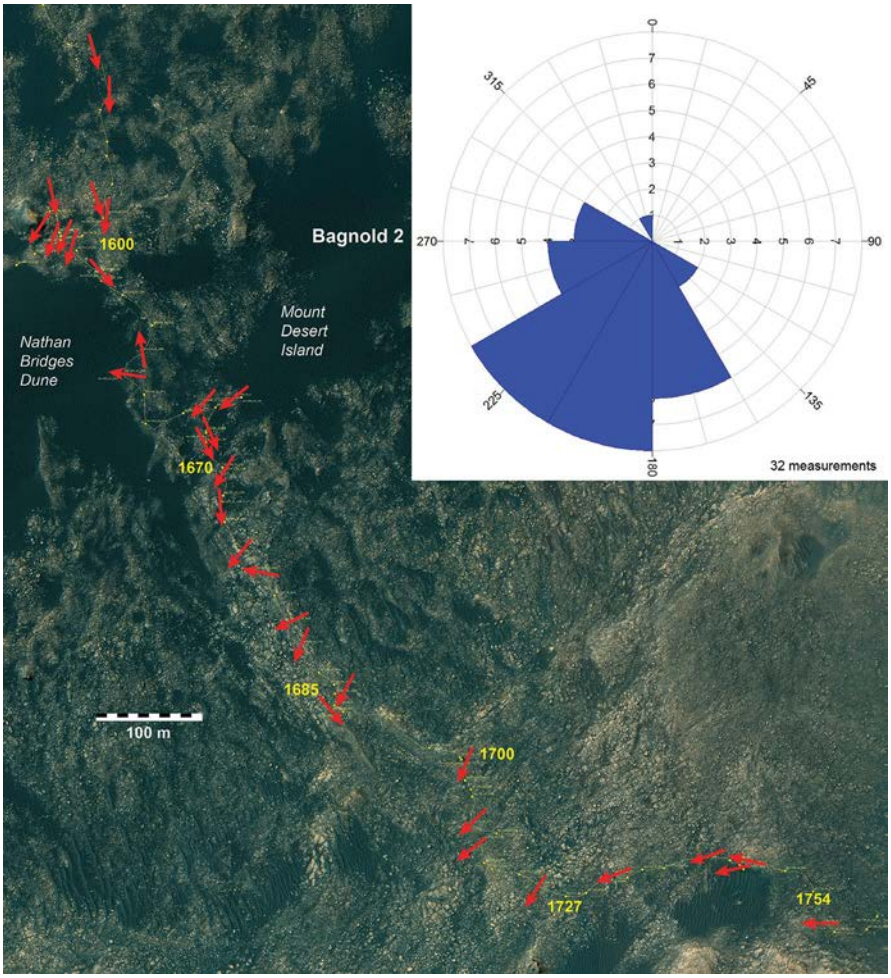

FIGURE 27 Region 'E' from Figure 22. Red arrows show wind directions derived from aeolian abrasion features imaged in MARDI images of mudstones. Dark areas are covered with actively moving sand dunes (Bagnold Dunes, investigation area 2). The identifiers "Mount Desert Island" and "Nathan Bridges dune" are from Lapotre and Rampe, 2018. The rose diagram shows the distribution of wind directions, and the numbers in yellow provide guidance on the time (Sol) the rover traversed these locations

(2014) in a study of ventifacts observed during the first year of rover operations. The rocks carrying ventifacts studied by Bridges *et al.* (2014) were sandstones, conglomerates and clasts liberated from conglomerates—rocks probably to be more abrasion resistant than mudstones, based on laboratory experiments described above. Bridges *et al.* (2014) suggested two formative wind regimes: one blowing to the southeast, and the other blowing to the northeast. The southeast direction is consistent with one of the two modern wind directions identified in the Bagnold Dunes from orbit (Silvestro *et al.*, 2013), whereas the northeast direction seen on the Naukluft Plateau (Figure 24) seems to have no modern equivalents and may record an older wind regime (Bridges *et al.*, 2014). Wind directions deduced from aeolian abrasion features collected on the VRR suggest that the concave (southward) indentation of the ridge served to focus airflow up and over the ridge, consistent with winds that generally blew towards the south as recorded by the majority of abrasion features (Figure 22).

4 | CONCLUSIONS

Laboratory abrasion experiments help identify analogous aeolian abrasion features in MSL MARDI images of Martian mudstone surfaces, and help interpret sand-driving wind azimuths along the rover traverse at Gale Crater. Orbital analyses of active ripple orientations, ripple movements and dune morphologies indicate the dominant direction of sand movement at the Bagnold Dunes is southwest (Silvestro *et al.*, 2013, 2016). However, this saltation direction coincides with ground abrasion measurements only within the generally southwest migration pathway of the Bagnold Dunes and closely associated active sand deposits. Outside of this area (i.e. in regions visited by MSL to the north and well to the south of the Bagnold Dunes), sand abrasion features in mudstone bedrock most commonly reflect saltation towards the south-southeast, with relatively wide variation around this azimuth. These south-southeast abrasion textures need not represent a different, past wind regime, however, because they are approximately aligned with winds toward the southeast that have been invoked to explain a secondary, 45° ripple crest orientation within the active Bagnold Dunes (Silvestro *et al.*, 2013). A simple interpretation combining this information involves: (a) wind events blowing southwest that are primarily responsible for southwest migration of the Bagnold Dunes have also caused bedrock abrasion of similar orientation between these dunes; and (b) less effective wind events (from an abrasion standpoint) blowing south-southeast have

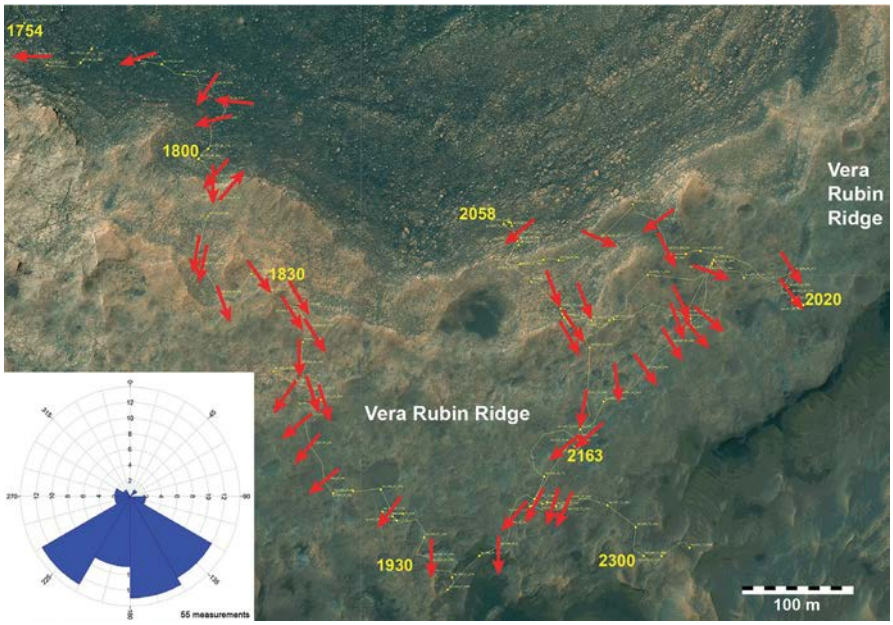

FIGURE 28 Region 'F' from Figure 22. Red arrows show sand abrasion directions measured in MARDI images of mudstones. The rose diagram shows the distribution of wind directions, and the numbers in yellow provide guidance on the time (Sol) the rover traversed these locations. Thin yellow line and yellow dots mark the rover traverse and rover stops respectively

broadly affected bedrock exposures elsewhere across the MSL landing site away from the Bagnold Dunes. The dominance of approximately S-SSE-SE abrasion textures in mudstone exposures away from the Bagnold Dunes migration pathway ultimately reflects a lack of competition from the effects of other wind directions and sand supply azimuths over these broad areas. In this regard, the southwest abrasion textures that are mostly restricted to mudstone exposures between dunes within the Bagnold dune field are an exception because of the availability of strong wind events blowing to the southwest combined with abundant nearby sand (dune) supplies immediately upwind. The short corridors between dunes should be subjected also to sand blowing S-SSE-SE as elsewhere along the MSL traverse, but at a much lesser rate than abrasive grain impacts from abundant sand blowing southwest between adjacent dunes. The higher rate of southwest abrasion of rock surfaces in these corridors obliterates the potential to preserve signatures there from lower-rate abrasion along other azimuths. Outside the corridors between individual Bagnold Dunes, the lack of southwest sand pathways indicated by abrasion orientations is consistent with a greater diffuse supply of sand somewhere upwind to the N-NNW-NW, rather than to the northeast.

The best case for preservation of an ancient sand-driving wind regime different from current wind and sediment supply conditions is represented by the northeast abrasion textures found on the Naukluft Plateau. These northeast abrasion textures, in more resistant sandstone materials, correspond to one of two abrasion directions measured in non-mudstone sedimentary rocks explored early in the MSL traverse that probably have similar, relatively high erosional resistance (Bridges *et al.*, 2014).

Besides natural variability in wind azimuth, factors contributing to abrasion direction variability include: (a) outcrop configurations can locally shield some outcrop faces from abrasion by sand from a dominant wind direction, and so restrict abrasion textures on such faces to form only from other, less pervasive wind directions where azimuths of access exist and (b) the upwind azimuths of available sand supply can vary over the exposure age of any given rock surface, especially in the nearby presence of an evolving, mobile dune field whose position and extent on the floor of Gale Crater relative to Mount Sharp might change over time. The record of aeolian abrasion preserved on the lower slopes of Mount Sharp indicates that sand supply and strong winds have coincided most consistently from northwest, north and northeast azimuths.

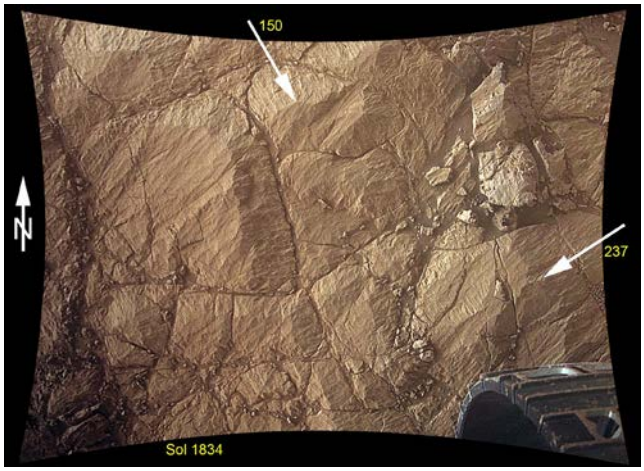

FIGURE 29 Aeolian abrasion on well-cemented VRR outcrop surface from Sol 1,834. There appear to be at least two well-represented directions at 150 and 237° (arrows). In situations like these no dominant wind direction was recorded. MARDI image 1834MD0007460000200792E01

Although surface geological features as well as interpreted past conditions show many parallels between Earth and Mars, the two planets nonetheless operate under different sets of boundary conditions. Therefore, and even though the same laws of physics and chemistry apply to both planets, exploring Mars allows us to 'see' aspects of geology that may be of miniscule importance on Earth (such as wind tails on mudstone surfaces) developed in great abundance and variety, as well as realizing that processes and features that we take for granted on Earth require special (and rare) sets of circumstances to occur on our planetary neighbour.

ACKNOWLEDGEMENTS

We are indebted to the Mars Science Laboratory Project engineering and science teams for their exceptionally skilled and diligent efforts in making the mission as effective as possible and enhancing science operations. We are also grateful to the MSL team members who participated in tactical and strategic operations. Without the support of both the engineering and science teams, the data presented here could not have been collected. This research was supported by NASA with contracts through the Jet Propulsion Laboratory to Malin Space Science Systems (1516826). The experimental portion of this research was partially supported by the sponsors of the Indiana University Shale Research Consortium (Anadarko, Chevron, ConocoPhillips, ExxonMobil, Shell, Statoil, Marathon, Whiting and Wintershall).

CONFLICT OF INTEREST

The authors have no conflict of interest to declare.

ORCID

Juergen Schieber https://orcid.org/0000-0003-0689-0780

REFERENCES

Bagnold, R.A. (1941) *The physics of blown sand and desert dunes*. London: Methuen, p. 265.

Banham, S.G., Gupta, S., Rubin, D.M., Watkins, J.A., Sumner, D.Y., Edgett, K.S. *et al*. (2018) Ancient Martian aeolian processes and palaeomorphology reconstructed from the Stimson formation on the lower slope of Aeolis Mons, Gale crater, Mars. *Sedimentology*, *65*, 993–1042.

Bennett, K.A., Edgett, K., Fey, D., Edgar, L.A., Fraeman, A., McBride, M.*et al*. (2018) Fine-scale textural observations at Vera Rubin Ridge, Gale crater, from the Mars Hand Lens Imager (MAHLI). Lunar and Planetary Science Conference, 49, abstract no. 1769.

Bibring, J.P. *et al*. (2006) Global mineralogical and aqueous mars history derived from OMEGA/Mars express data. *Science*, *312*, 400–404.

Bridges, Nathan and Ehlmann, Bethany (2017) The Mars Science Laboratory (MSL) Bagnold Dunes Campaign, Phase I: overview and introduction to the special issue. *Journal of Geophysical Research: Planets*, *123*, 3–19. https://doi.org/10.1002/2017je005401

Bridges, N.T., Greeley, R., Haldemann, A.F.C., Herkenhoff, K.E., Kraft, M., Parker, T.J. *et al*. (1999) Ventifacts at the Pathfinder landing site. *Journal of Geophysical Research: Planets*, *104*(E4), 8595–8615. https://doi.org/10.1029/98JE02550

Bridges, N.T., Laity, J.E., Greeley, R., Phoreman, J. and Eddlemon, E.E. (2004) Insights on rock abrasion and ventifact formation from laboratory and field analog studies with applications to Mars. *Planetary and Space Science*, *52*, 199–213. https://doi.org/10.1016/j.pss.2003.08.026

Bridges, N.T., Calef, F.J., Hallet, B., Herkenhoff, K.E., Lanza, N.L., Le Mouelic, S. *et al*. (2014) The rock abrasion record at Gale Crater: Mars Science Laboratory results from Bradbury Landing to Rocknest. *Journal of Geophysical Research: Planets*, *119*, 1374–1389. https://doi.org/10.1002/2013JE004579

Calef, F.J. III and Parker, T. (2016) MSL Gale Merged Orthophoto Mosaic, Publisher: PDS Annex, U.S. Geological Survey, http://bit.ly/MSL_Basemap

Calef, F.J. III and Parker, T. (2016) MSL Gale Merged Orthophoto Mosaic, Publisher: PDS Annex, U.S. Geological Survey, http://bit.ly/MSL_Basemap

Carr, M.H. (1996) *Water on mars*. New York, NY: Oxford University Press, 229 pp.

Carr, M.H. and Head, J.W. (2010) Geologic history of Mars. *Earth and Planetary Science Letters*, *294*, 185–203. https://doi.org/10.1016/j.epsl.2009.06.042

Day, M. and Kocurek, G.A. (2016) Observations of an aeolian landscape: from surface to orbit in Gale Crater. *Icarus*, *280*, 37–71.

Edgett, K.S., Yingst, R.A., Ravine, M.A., Caplinger, M.A., Maki, J.N., Ghaemi, F.T. *et al*. (2012) Curiosity's Mars Hand Lens Imager (MAHLI) investigation. *Space Science Reviews*, *170*, 259–317. https://doi.org/10.1007/s11214-012-9910-4

Favaro, E.A., Hugenholtz, C.H. and Barchyn, T.E. (2017) Evolution and diagnostic utility of aeolian rat-tails: a new type of abrasion feature on Earth and Mars. *Aeolian Research*, *28*, 91–98. https://doi.org/10.1016/j.aeolia.2017.08.004

Fedo, C.M., Grotzinger, J. P., Gupta, S., Stein, N.T., Watkins, J., Banham, S. *et al*. (2017) Facies analysis and basin architecture of the upper part of the Murray Formation, Gale Crater, Mars. 48th Lunar and Planetary Sciences Conference, Houston, March 20–24 2017, abstract no. 1689.

Fraeman, A.A., Arvidson, R.E., Catalano, J.G., Grotzinger, J.P., Morris, R.V., Murchie, S.L. *et al*. (2013) A hematite-bearing layer in Gale Crater, Mars: mapping and implications for past aqueous conditions. *Geology*, *41*, 1103–1106.

Fraeman, A.A., Edgar, L.A., Grotzinger, J.P., Vasavada, A.R., Johnson, J.R., Wellington, D.F.*et al*. (2018) Curiosity's investigation at Vera Rubin Ridge. Lunar and Planetary Science Conference, 49, abstract #1557.

Gómez-Elvira, J., Armiens, C., Castañer, L., Domínguez, M., Genzer, M., Gómez, F. *et al*. (2012) REMS: the environmental sensor suite for the Mars Science Laboratory rover. *Space Science Reviews*, *170*(1–4), 583–640.

Greeley, R., Bridges, N.T., Kuzmin, R.O. and Laity, J.E. (2002) Terrestrial analogs to wind-related features at the Viking and Pathfinder landing sites on Mars. *Journal of Geophysical Research*, *107*(E1), 5005. https://doi.org/10.1029/2000JE001481

Greeley, R., Squyres, S.W., Arvidson, R.E., Bartlett, P., Bell, J.F. III, Blaney, D. *et al*. (2004) Wind-related processes detected by the Spirit rover at Gusev Crater, Mars. *Science*, *305*, 810–821. https://doi.org/10.1126/science.1100108

Greeley, R., Arvidson, R.E., Barlett, P.W., Blaney, D., Cabrol, N.A., Christensen, P.R. *et al*. (2006) Gusev crater: Wind-related features and processes observed by the Mars Exploration Rover Spirit. *Journal of Geophysical Research: Planets*, *111*, E02S09. doi: https://doi.org/10.1029/2005JE002491

Greeley, R., Whelley, P.L., Neakrase, L.D.V., Arvidson, R.E., Bridges, N.T., Cabrol, N.A. *et al*. (2008) Columbia Hills, Mars: Aeolian features seen from the ground and orbit. *Journal of Geophysical Research*, *113*, E06S06. https://doi.org/10.1029/2007JE002971

Grotzinger, J.P. *et al*. (2014) A habitable fluvio-lacustrine environment at Yellowknife Bay, Gale Crater, Mars. *Science*, *343*(6169), 1242777

Grotzinger, J.P., Crisp, J., Vasavada, A.R., Anderson, R.C., Baker, C.J., Barry, R. *et al*. (2012) Mars Science Laboratory mission and science investigation. *Space Science Reviews*, *170*, 5–56. https://doi.org/10.1007/s11214-012-9892-2

Grotzinger, J.P., Gupta, S., Malin, M.C., Rubin, D.M., Schieber, J., Siebach, K. *et al*. (2015) Deposition, exhumation, and paleoclimate of an ancient lake deposit, Gale crater, Mars. *Science*, *350*(6257), aac7575–aac7575. October 2015.

Herkenhoff, K.E., Grotzinger, J., Knoll, A.H., McLennan, S.M., Weitz, C. and Yingst, A. *et al*. (2008) Surface processes recorded by rocks and soils on Meridiani Planum, Mars: microscopic Imager observations during opportunity's first three extended missions. *Journal of Geophysical Research*, *113*, E12S32.

Howald, T.V. and Schieber, J. (2008) Textural features produced by aeolian erosion of mudstones. 39th Lunar and Planetary Sciences Conference, Houston, March 10-14 st 2008, Abstract No. 2052, Abstract Volume – CD. https://www.lpi.usra.edu/meetings/lpsc2008/pdf/2052.pdf

Laity, J.E. (1994) Landforms of aeolian erosion. In: Abrahams, A.D. and Parsons, A.J. (Eds.) *Geomorphology of Desert Environments*. London: Chapman & Hall, pp. 506–535.

Laity, J.E. (2009) Landforms, landscapes, and processes of aeolian erosion. In: Parsons, A.J. and Abrahams, A.D. (Eds.), *Geomorphology of Desert Environments*, 2nd edition, Springer Netherlands: Springer Science+Business Media. doi: 10.1007/978-1-4020-5719-9, Chapter 19, pp. 597–627.

Laity, J.E. (2011) Wind erosion in drylands. In: Thomas, D.S.G. (Ed.) *Arid Zone Geomorphology: Process, Form and Change in Drylands*, 3rd edition. West Sussex, UK: Wiley-Blackwell, pp. 539–568.

Laity, J.E. and Bridges, N.T. (2009) Ventifacts on Earth and Mars: Analytical, field, and laboratory studies supporting sand abrasion and windward feature development. *Geomorphology*, *105*, 202–217. https://doi.org/10.1016/j.geomorph.2008.09.014

Lancaster, N. (1984) Characteristics and occurrence of wind erosion features in the Namib desert. *Earth Surface Processes and Landforms*, *9*, 469–478.

Lapôtre, M.G.A and Rampe, E.B. (2018) Curiosity's investigation of the Bagnold Dunes, Gale Crater: overview of the two-phase scientific campaign and introduction to the special collection. *Geophysical Research Letters*, *45*, 10200–10210. https://doi.org/10.1029/2018GL079032

Malin, M.C. and Edgett, K. (2000) Sedimentary rocks of early mars. *Science*, *290*, 1927–1937. https://doi.org/10.1126/science.290.5498.1927

Malin, M.C., Ravine, M.A., Caplinger, M.A., Ghaemi, F.T., Schaffner, J.A., Maki, J.N. *et al*. (2017) The Mars Science Laboratory (MSL) Mast cameras and Descent imager: I. Investigation and instrument descriptions. *Earth and Space Sciences*, *4*, 506–539. https://doi.org/10.1002/2016EA000252

Maxson, J.H. (1940) Fluting and faceting of rock fragments. *Journal of Geology*, *48*, 717–751.

McEwen, A.S., Eliason, E.M., Bergstrom, J.W., Bridges, N.T., Hansen, C.J. and Delamere, W.A. *et al*. (2007) Mars reconnaissance orbiter's high resolution imaging science experiment (HiRISE). *Journal of Geophysical Research*, *112*, EO5SO2. https://doi.org/10.1029/2005JE002605

Minitti, M.E., Kennedy, M.R., Krezoski, G.M., Rowland, S.K., Schieber, J., Stack, K.M. and Yingst, R.A. (2017) Using MARDI twilight images to assess variations in the Murray formation with elevation, Gale crater, Mars. Lunar Planetary Science Conference 48, Abstract #2622.

Minitti, M.E., Malin, M.C., Van Beek, J.K., Caplinger, M., Maki, J.N., Ravine, M. *et al*. (2019) Distribution of primary and secondary features in the Pahrump Hills outcrop (Gale crater, Mars) as seen in a Mars Descent Imager (MARDI) "sidewalk" mosaic. *Icarus*, *328*, 194–209. https://doi.org/10.1016/j.icarus.2019.03.005

Moores, J.E., Schieber, J., Kling, A.M., Haberle, R.M., Moore, C.A. and Anderson, M.S. *et al*. (2016) Transient atmospheric effects of the landing of the Mars Science Laboratory Rover: The emission and dissipation of dust and carbazic acid. *Advances in Space Research*, *58*, 1066–1092.

Parker, T.J., Calef, F.J., Golombek, M.P. and Hare, T.M. (2012) High-resolution basemaps for localization, mission planning, and geologic mapping at Meridiani Planum and Gale crater. Lunar and Planetary Science Conference 43, abstract 2535.

Rampe, E.B., Ming, D.W., Blake, D.F., Bristow, T.F., Chipera, S.J., Grotzinger, J.P. *et al*. (2017) Mineralogy of an ancient lacustrine mudstone succession from the Murray formation, Gale crater, Mars. *Earth and Planetary Science Letters*, *471*, 172–185. https://doi.org/10.1016/j.epsl.2017.04.021

Reineck, H.E. and Singh, I.B. (1980) *Depositional Sedimentary Environments*. New York, NY: Springer-Verlag, 551 pp.

Rivera-Hernandez, F., Sumner, D.Y., Mangold, N., Banham, S.G., Edgett, K.S., Fedo, C.M., *et al*. (2019) Vera Rubin Ridge (Gale Crater, Mars) grain size observations from ChemCam LIBS data and interpretations. 50th Lunar and Planetary Sciences Conference, Houston, March 18–22, 2019, abstract no. 3029, Abstract Volume – CD.

Rossman, B., Wilson, R. and Schieber, J. (2012) Eolian erosion experiments on soft sedimentary rocks – measurement of erosion rates, textural observations, and implications for Mars Rover geology. 43rd Lunar and Planetary Sciences Conference, Houston, March 19–23 2012, abstract no. 2837, Abstract Volume – CD.

Schieber, J., Bish, D., Coleman, M., Reed, M., Hausrath, E.M., Cosgrove, J. *et al*. (2017) Encounters with an unearthly mudstone: understanding the first mudstone found on Mars. *Sedimentology*, *64*, 311–358.

Sharp, R.P. (1949) Pleistocene ventifacts east of the Big Horn Mountains, Wyoming. *The Journal of Geology*, *57*(2), 175–195. https://doi.org/10.1086/625596

Sharp, R.P. and Malin, M.C. (1984) Surface geology from Viking landers: A second look. *Geological Society of America Bulletin*, *95*, 1398–1412. https://doi.org/10.1130/0016-7606(1984)95<1398:SGFVLO>2.0.CO;2

Silvestro, S., Vaz, D.A., Ewing, R.C., Rossi, A.P., Fenton, L.K., Michaels, T.I. *et al*. (2013) Pervasive aeolian activity along rover

Curiosity's traverse in Gale crater, Mars. *Geology*, *41*(4), 483–486. https://doi.org/10.1130/G34162.1

Silvestro, S., Vaz, D.A., Yizhaq, H. and Esposito, F. (2016) Dune-like dynamic of Martian aeolian large ripples. *Geophysical Research Letters*, *43*, https://doi.org/10.1002/2016GL070014

Sullivan, R., Banfield, D., Bell, J.F. III, Calvin, W., Fike, D., Golombek, M. *et al*. (2005) Aeolian processes at the Mars Exploration Rover Meridiani Planum landing site. *Nature*, *436*, 58–61. https://doi.org/10.1038/nature03641

Thomas, M., Clarke, J.D.A. and Pain, C.F. (2005) Weathering, erosion and landscape processes on Mars identified from recent rover imagery, and possible Earth analogs. *Australian Journal of Earth Sciences*, *52*, 365–378.

Thomson, B.J., Bridges, N.T. and Greeley, R. (2008) Rock abrasion features in the Columbia Hills, Mars. *Journal of Geophysical Research: Planets*, *113*, E08010. https://doi.org/10.1029/2007JE003018

Urso, A., Chojnacki, M. and Vaz, D.A. (2018) Dune-yardang interactions in Becquerel crater, Mars. *Journal of Geophysical Research: Planets*, *123*, 353–368. https://doi.org/10.1002/2017JE005465

Viúdez-Moreiras, D., Gómez-Elvira, J., Newman, C.E., Navarro, S., Marin, M., Torres, J. *et al*. (2019a) Gale surface wind characterization based on the Mars Science Laboratory REMS dataset. Part I: Wind retrieval and Gale's wind speeds and directions. *Icarus*, *319*, 909–925.

Viúdez-Moreiras, D., Gómez-Elvira, J., Newman, C.E., Navarro, S., Marina, M., Torres, J. *et al*. (2019b) Gale surface wind characterization based on the Mars Science Laboratory REMS dataset. Part II: Wind probability distributions. *Icarus*, *319*, 645–656.

Wilson, R., Schieber, J. and Howald, T. (2011). Experimental Eolian erosion of soft sedimentary rocks with a variety of abrasives –- observed features and potential applications for Mars Rover Geology. 42nd Lunar and Planetary Sciences Conference, Houston, March 7–11 2011, Abstract No. 2176, Abstract Volume – CD.

Yen, A.S., Gellert, R., Schröder, C., Morris, R.V., Bell, J.F. III, Knudson, A.T. *et al*. (2005) An integrated view of the chemistry and mineralogy of martian soils. *Nature*, *436*, 49–54. https://doi.org/10.1038/nature03637

Yingst, R.A., Kah, L.C., Palucis, M., Williams, R.M.E., Garvin, J. and Bridges, J.C. *et al*. (2013) Characteristics of pebble- and cobble-sized clasts along the Curiosity rover traverse from Bradbury Landing to Rocknest. *Journal of Geophysical Research: Planets*, *118*, 2361–2380.

How to cite this article: Schieber J, Minitti ME, Sullivan R, et al. Engraved on the rocks—Aeolian abrasion of Martian mudstone exposures and their relationship to modern wind patterns in Gale Crater, Mars. *Depositional Rec*. 2020;6:625–647. https://doi.org/10.1002/dep2.110